# β-catenin regulates FOXP2 transcriptional activity via multiple binding sites

Gesa Richter[1,*], Tianshu Gui[2], Benjamin Bourgeois[1], Chintan N. Koyani[1,3], Peter Ulz[4], Ellen Heitzer[4], Dirk von Lewinski[3], Boudewijn M. T. Burgering[2], Ernst Malle[1] and Tobias Madl[1,5]

1 Gottfried Schatz Research Center for Cell Signaling, Metabolism and Aging, Molecular Biology and Biochemistry, Medical University of Graz, Austria
2 Oncode Institute and Department of Molecular Cancer Research, Center for Molecular Medicine, University Medical Center Utrecht, The Netherlands
3 Division of Cardiology, Department of Internal Medicine, Medical University of Graz, Austria
4 Institute of Human Genetics, Diagnostic and Research Center for Molecular BioMedicine, Medical University of Graz, Austria
5 BioTechMed, Graz, Austria

The transcription factor forkhead box protein P2 (FOXP2) is a highly conserved key regulator of embryonal development. The molecular mechanisms of how FOXP2 regulates embryonal development, however, remain elusive. Using RNA sequencing, we identified the Wnt signaling pathway as key target of FOXP2-dependent transcriptional regulation. Using cell-based assays, we show that FOXP2 transcriptional activity is regulated by the Wnt coregulator β-catenin and that β-catenin contacts multiple regions within FOXP2. Using nuclear magnetic resonance spectroscopy, we uncovered the molecular details of these interactions. β-catenin contacts a disordered FOXP2 region with α-helical propensity via its folded armadillo domain, whereas the intrinsically disordered β-catenin N terminus and C terminus bind to the conserved FOXP2 DNA-binding domain. Using RNA sequencing, we confirmed that β-catenin indeed regulates transcriptional activity of FOXP2 and that the FOXP2 α-helical motif acts as a key regulatory element of FOXP2 transcriptional activity. Taken together, our findings provide first insight into novel regulatory interactions and help to understand the intricate mechanisms of FOXP2 function and (mis)-regulation in embryonal development and human diseases.

**Database**
Expression data are available in the GEO database under the accession number GSE138938.

**Abbreviations**
ChIP-Seq, chromatin immunoprecipitation sequencing; DEGs, differentially expressed genes; FH, forkhead domain; FOXP2, forkhead box protein P2; GO, Gene Ontology; IDR, intrinsically disordered region; IPTG, isopropyl β-D-1-thiogalactopyranoside; KEGG, Kyoto Encyclopedia of Genes and Genomes; MAPK, mitogen-activated protein kinase; NF, nuclear factor; NMR, nuclear magnetic resonance; RNA-Seq, RNA sequencing; STAT3, signal transducer and activator of transcription 3; StAx, stapled Axin; TBST, tris-buffered saline containing Tween 20; TCEP, tris(2-carboxyethyl) phosphine; TCF/LEF, T-cell factor/lymphoid enhancer-binding factor; TCF7L2, also known as TCF4, transcription factor 7-like 2; TEV, tobacco etch virus; TNF, tumor necrosis factor; U2OS, human osteosarcoma epithelial cell line.

## Introduction

The transcription factor FOXP2 has been discovered as functional element of human speech development [1]. FOXP2 belongs to the most conserved proteins in mammals [2], and its function in neuronal and embryonal development, vocalization, and social behavior has been investigated in various functional animal studies [3–7]. Dual transcriptional roles have been reported for FOXP2, both in transcriptional repression [8,9], and in activation of target genes [10].

Most of the recent studies focused on FOXP2 targets involved in neuronal cells or brain tissue in order to reveal the role of FOXP2 in human speech development. Up to now, more than 1000 direct or indirect targets have been found using chromatin immunoprecipitation sequencing (ChIP-Seq), ChIP-chip (chromatin immunoprecipitation coupled with hybridization to promoter microarrays), microarray, and RNA sequencing (RNA-Seq) [6,9–16]. Multiple pathways are regulated by FOXP2, including activation of mitogen-activated protein kinase (MAPK), and signaling pathways such as notch, retinoic acid, insulin-growth factor, signal transducer and activator of transcription 3 (STAT3), p53, sonic hedgehog, and Wnt/β-catenin [9,10,17,18].

FOXP2 is associated with various biological functions. Therefore, it is not surprising that FOXP2 dysfunctions are associated with a broad range of diseases such as developmental verbal dyspraxia [19], autism [20], and various cancer types, including ovarian, hepatocellular, bone, gastric, breast, prostate, and colorectal cancer [21]. Dysregulation of FOXP2 might play a crucial role in cancer initiation and progression and is considered as diagnostic marker of neoplastic cells [21]. Due to the key role of FOXP2 in a plethora of biological pathways, tight regulation of FOXP2 transcriptional activity is essential. However, the molecular mechanisms underlying regulation of FOXP2 transcriptional activity remain elusive.

To better understand the regulatory mechanisms, which control the transcriptional activity of FOXP2, we aimed to find clues about candidate pathways, which are regulated by FOXP2 to get ideas about regulatory elements, motifs, and processes in cells. Recent studies have identified a potential link between FOXP proteins and the Wnt signaling pathway [22,23]. Therefore, in this report, we investigated a possible link between FOXP2 and the Wnt pathway, as both are important in embryonal development and might regulate each other. Thus, we focused on the interaction with β-catenin as transcriptional coactivator, which is regulating, when active, various transcription factors such as T-cell factor/lymphoid enhancer-binding factor (TCF/LEF) [24–26], hypoxia-induced factor 1 α under hypoxic conditions [27], or FOXO under oxidative stress [28]. Using a combination of complementary *in vitro* and cell-based approaches, we revealed the role of β-catenin as functional regulator of FOXP2 transcriptional activity. Our results suggest that additional factors such as the structure and composition of FOXP2 DNA target motifs, binding of cofactors, and/or post-translational modifications play an important role in FOXP2-mediated transcriptional regulation.

## Results and Discussion

### FOXP2 regulates multiple genes and pathways

Up to now, the complex FOXP2-mediated regulatory mechanisms and its implications in biological functions remain elusive. To determine possible regulatory elements, which are controlled by FOXP2, we performed RNA-Seq experiments with a human osteosarcoma epithelial cell line (U2OS) overexpressing wild-type human FOXP2 (Fig. 1A). Functional enrichment analysis was performed for all differentially expressed genes (DEGs). By comparing the Mock-transfected cells as controls with cells overexpressing FOXP2, we found 3054 genes to be significantly upregulated and

**Fig. 1.** Multiple genes and pathways such as Wnt signaling are regulated by FOXP2. (A) Western blot showing the overexpression of FOXP2 in U2OS cells. Lane 1 is lysate of mock-transfected cells as control. Lane 2 is total cell protein lysate of FOXP2-overexpressing cells. One representative blot out of three is shown (*n* = 3). (B) Volcano plot shows distribution of significantly up- (red dots) and downregulated (blue dots) genes upon FOXP2 overexpression in U2OS cells. Genes with a fold change (FC) (log2) below 1 or above −1 are shown in black as not significant. Not significantly change genes with a *P*-value > 0.05 are not shown. (C) Top 15 of significantly enriched KEGG pathways of up- and downregulated genes upon FOXP2 overexpression in U2OS cells. Red dotted line indicates cutoff (*P*-value: 0.05). (D) Top 15 of significantly enriched GO term biological functions of up- and downregulated genes upon FOXP2 overexpression in U2OS cells. Red dotted line indicates cutoff (*P*-value: 0.05). (E) Schematic representation of the canonical Wnt/β-catenin pathway. ON and OFF mean Wnt pathway active or inactive, respectively. (F) mRNA expression plot and heatmap of Wnt target genes in FOXP2-overexpressing cells compared with control cells as log2 fold change, genes are represented in a range of red (upregulated) and blue (downregulated) (*n* = 5) (G) Validation of selection of Wnt targets by qPCR. Data are shown as mean ± SEM, *n* = 5.
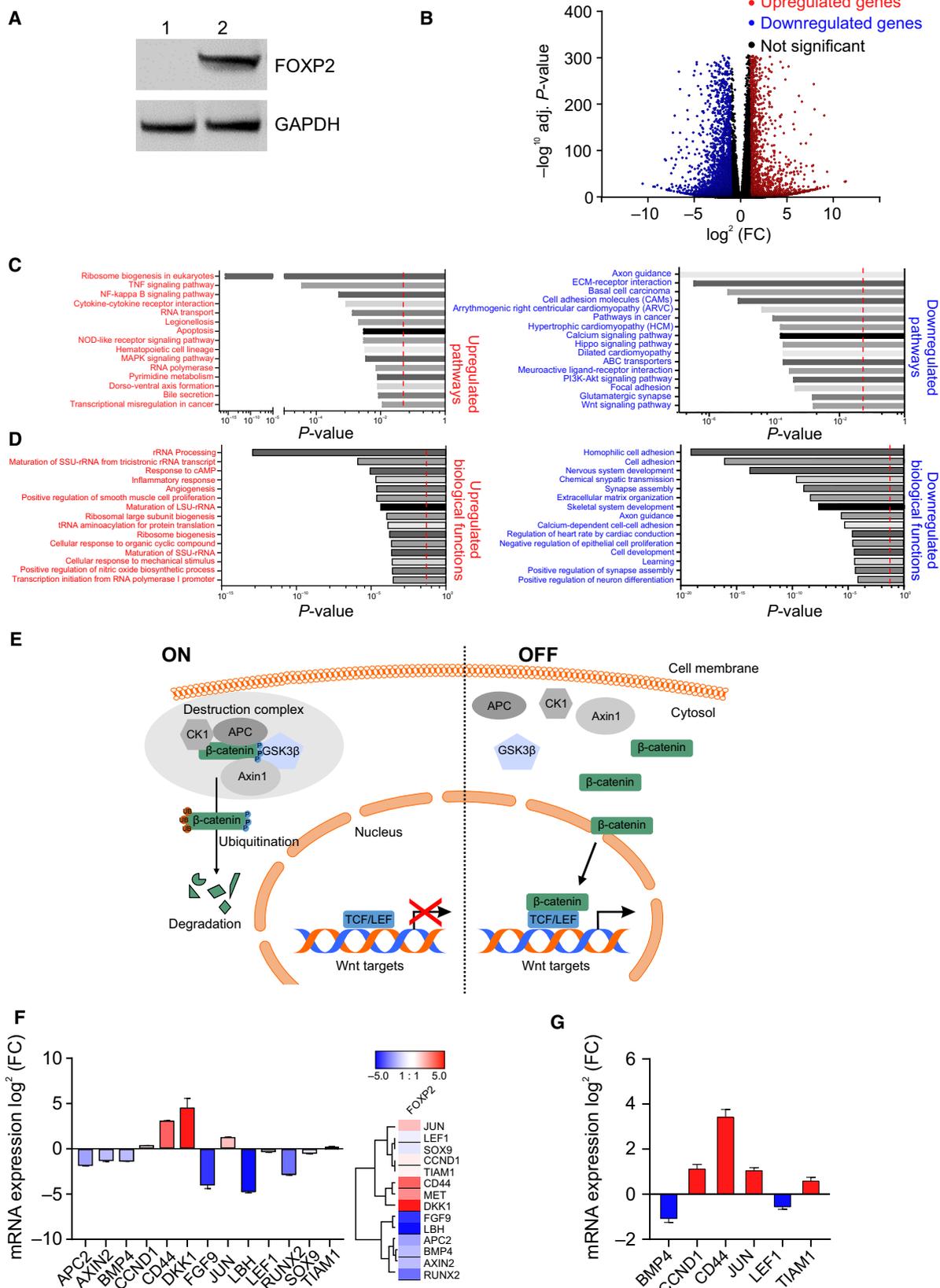
4555 genes to be downregulated (Fig. 1B). This is in line with previous studies, demonstrating that FOXP2 can act both as transcriptional activator and as repressor [8,9]. In order to obtain a functional interpretation of the changed gene expression profiles, we performed Gene Ontology (GO) and Kyoto Encyclopedia of Genes and Genomes (KEGG) analysis based on Fisher's extract test and using DAVID 3.8 [29].

KEGG pathway analysis showed that the 3054 upregulated genes were enriched in 47 pathways, and GO analysis revealed 233 biological functions. The 4555 downregulated genes were associated with 49 pathways (KEGG) and 378 biological functions (GO term). The 15 most significant KEGG pathways of up- and downregulated genes and biological functions are shown in Fig. 1C,D, respectively. In line with a previous study using ChIP-chip [6], we find Axon guidance, the Wnt and the MAPK signaling pathways to be regulated by FOXP2. Interestingly, our data show that FOXP2 overexpression leads to yet unknown changes in several additional pathways such as cell adhesion molecules, tumor necrosis factor (TNF)-signaling, calcium signaling, and Hippo signaling (Fig. 1C). Thus, FOXP2 regulates a broad range of biological functions and plays a crucial role in signal transduction [21].

The most downregulated pathway in our analysis is Axon guidance, which is consistent with previous results obtained from ChIP-chip [6] and highlights the key role of FOXP2 in neural development and neurotransmission. Furthermore, we confirm the role of FOXP2 in regulation of pathways important in brain development and morphology, memory, and learning [30], such as cell adhesion molecules, Hippo signaling, and Wnt signaling [31–33]. The second most significantly upregulated pathway is the TNF signaling pathway followed by nuclear factor (NF)-kappa β signaling pathway. TNF signaling activates the NF-kappa β transcription factor [34] and the MAPK signaling pathway and thereby regulates apoptosis [35,36]. So far no direct link between TNF/NF-kappa β signaling and FOXP2 has been found, although one study found different expression levels of the *FOXP2* gene in rheumatoid arthritis patients undergoing an anti-TNF therapy [34]. Given that a link between FOXP3 with NF-kappa β signaling has been reported [37], our data suggest FOXP2 as an additional regulator of TNF/NF-kappa β signaling in analogy to

FOXP3. Interestingly, pathways linked to cancer appeared in both up- and downregulated DEGs. This can be explained that FOXP2 has the capacity to repress both pro-oncogenic and tumor suppressor genes depending on the cancer [21].
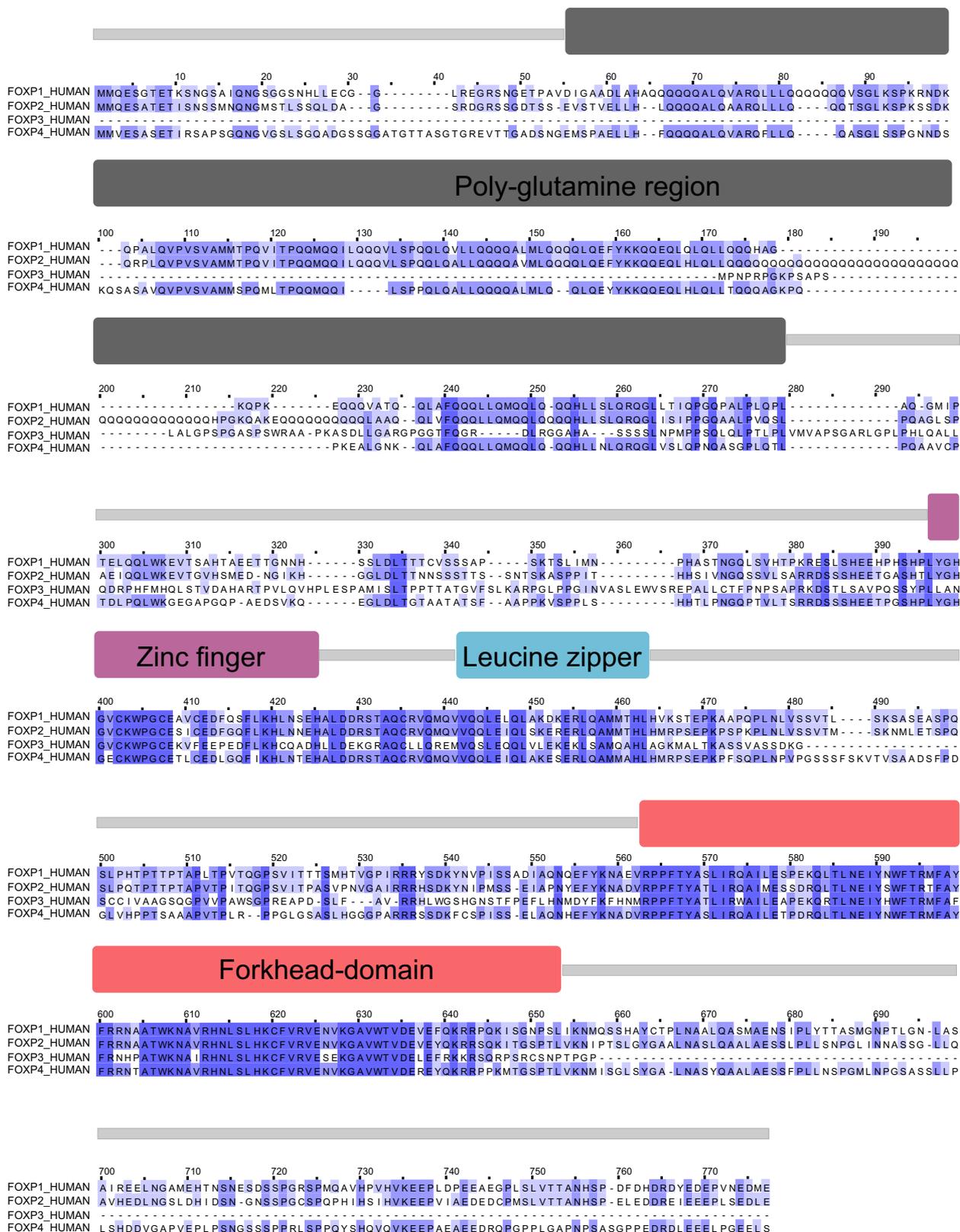
## FOXP2 mediates transcription of Wnt target genes

Interestingly, Wnt signaling-related GO terms appeared in five biological functions in the set of downregulated genes, including 'Wnt signaling pathway' (*P*-value: 0.0013), 'negative regulation of Wnt signaling pathway' (*P*-value: 0.0083), 'negative regulation of canonical Wnt signaling pathway' (*P*-value: 0.021), 'Wnt signaling pathway, calcium modulating pathway' (*P*-value: 0.033), and 'positive regulation of Wnt signaling pathway, planar cell polarity pathway' (*P*-value: 0.058). Additionally, Wnt signaling appears in the 15 most downregulated KEGG pathways, indicating that FOXP2 plays an important role in downregulating genes related to the Wnt signaling pathway.

Wnt signaling operates in both vertebrates and invertebrates [38] and acts as central regulatory element in a remarkably diverse range of functions during embryonic development and adult homeostasis controlling cell fate specification, cell proliferation, and cell migration [39–41]. Disruptions in this highly conserved signaling pathway result in various diseases including cancer and neurodegenerative diseases [39,42–44]. In the inactive state of the Wnt signaling pathway, a large multiprotein complex called the β-catenin destruction complex traps and degrades the coactivator β-catenin in the cytoplasm, preventing its translocation to the nucleus (Fig. 1E). In the active state, the destruction complex no longer degrades β-catenin, leading to higher cytosolic levels, its nuclear translocation, activation of the T-cell factor/lymphoid enhancer-binding factor (TCF/LEF) family of transcription factors, and transcription of Wnt target genes [24–26].

To reveal the effect of FOXP2 on the Wnt signaling pathway, we analyzed the expression of 14 known Wnt target genes in our RNA-Seq data set and visualized it via a heatmap (Fig. 1F). FOXP2 overexpression significantly changes the expression of all observed Wnt targets providing first evidence for FOXP2 function in the regulation of the Wnt pathway. To validate

**Fig. 2.** Sequence alignment of FOXP1 (UNIProtKB–Q9H334), FOXP2 (UNIProtKB–O15409), FOXP3 (UNIProtKB–Q9BZS1), and FOXP4 (UNIProtKB–Q8IVH2), using CLUSTAL OMEGA (EMBL-EBI, HINKSTON, UK). Blue color indicates conservation of residues. Above alignment structural organization of FOXP2 is shown for visualization of domains of FOXP2.

**Poly-glutamine region**

**Zinc finger**

**Leucine zipper**

**Forkhead-domain**

FOXP1_HUMAN
FOXP2_HUMAN
FOXP3_HUMAN
FOXP4_HUMAN

the gene expression changes from the RNA-Seq data, we performed qPCR of known Wnt targets (Fig. 1G). The expression levels of the selected genes were in agreement with the RNA-Seq data and thus validate the effect of FOXP2 overexpression on the regulation of the Wnt pathway.

Regulation of the Wnt pathway has been reported for other members of the FOXP family [22,23]. The human FOXP family consists of four members, FOXP1, FOXP2, FOXP3, and FOXP4. On the molecular level, FOXP1, FOXP3, and FOXP4 share many similarities compared with FOXP2 (sequence alignment in Fig. 2). The most conserved domains among FOXP proteins are the DNA-binding forkhead domain (FH), the zinc finger, and the leucine zipper. Using mass spectrometry, Walker *et al.* [22] showed that FOXP1 forms a complex with β-catenin, transcription factor 7-like 2 (TCF7L2, also known as TCF4), and CREP-binding protein (CBP) and thereby enhances expression of Wnt target genes such as *AXIN2* or *NKD1*. FOXP3 misregulation is linked to Wnt pathway activation in lung cancer by promoting tumor growth and metastasis [23]. FOXP3 was reported to interact with β-catenin via coimmunoprecipitation and to be transcriptionally regulated by β-catenin in DNA-microarray [45]. Until now, however, it remains elusive whether FOXP2 is regulated by β-catenin, and whether regulation of FOXP proteins is due to a direct interaction with β-catenin.

## β-catenin interacts with FOXP2 and regulates its transcriptional activity

We therefore aimed to address first whether the FOXP2-mediated regulation of the Wnt pathway is mediated by an interaction of FOXP2 with β-catenin. Indeed, we found that FOXP2 coimmunoprecipitates with β-catenin at endogenous levels in HEK 293T cells that endogenously express both proteins, using either FOXP2 or β-catenin as bait (Fig. 3A). This indicates that both proteins interact directly or indirectly like in the case of FOXP1 [22] and FOXP3 [23] and that in

turn β-catenin could regulate FOXP2 activity through this interaction.

To investigate the effect of β-catenin on FOXP2 transcriptional activity, we then performed RNA-Seq analysis to determine changes in gene expression profiles upon β-catenin activation. In this approach, we used U2OS cells, which express a cytosolic, transcriptionally inactive form of β-catenin [46] but do not express FOXP2 protein. Treatment of U2OS cells with the Wnt/β-catenin pathway activator CHIR (99021; Tocris, Bio-Techne Ltd., Abington, UK), a GSK3β inhibitor, showed efficient translocation of β-catenin into the nucleus, as reported previously [47] (Fig. 3B). Using mock-transfected cells as control, we compared the gene expression to cells which (a) overexpressed FOXP2, (b) were treated only with CHIR, and (c) overexpressed FOXP2 and were treated with CHIR. Overlap of significantly DEGs within all conditions is represented in Fig. 3C as Venn diagram. The top 5 most significant KEGG pathways for each group are listed in Fig. 3D.

We then focused our data analysis on the set of genes selectively and significantly affected by β-catenin activation upon CHIR treatment in a context of FOXP2 overexpression. Those genes highlight specific pathways regulated by both FOXP2 and β-catenin and represent the most populated group with 1913 significantly upregulated genes. This confirms a mechanistic correlation between FOXP2 and β-catenin in the regulation of gene transcription. KEGG pathway and GO term analysis revealed that those 1913 genes were enriched in eight KEGG pathways (top 5 shown in Fig. 3D) and 38 biological functions (top 15 in Fig. 3E). Those pathways are associated with β-catenin-dependent regulation of FOXP2 transcriptional activity as they do not appear in the conditions of FOXP2 overexpression only and in CHIR treatment only.

Furthermore, we investigated the genes downregulated under the experimental conditions (Fig. 3C) in order to see the role of β-catenin in the FOXP2-dependent inhibition of gene expression. The fractions with

**Fig. 3.** β-catenin interacts with FOXP2 and regulates its transcriptional activity. (A) Co-IP of endogenous FOXP2 and β-catenin from HEK-293-T cells shows interaction. Control shows no unspecific binding of both proteins to the beads. One representative blot out of three is shown ($n = 3$). (B) Western blot showing the cellular localization of β-catenin in U2OS cells upon treatment of reagent CHIR inducing increased nuclear translocation of β-catenin. Lane 1 = control cells, 2 = CHIR 99021 (5 μM). Loading controls: nuclear fraction = Lamin, cytosolic fraction = GAPDH. One representative blot out of three is shown ($n = 3$) (C) Venn diagram showing overlap of DEGs in FOXP2-overexpressing cells, CHIR-treated cells, and FOXP2-overexpressing cells treated with CHIR. (D) Top 5 of significantly changes KEGG pathways of up- and downregulated genes of each condition of DEGs. (E) Top 15 of significantly enriched GO term biological functions of up- and downregulated genes upon FOXP2 overexpression plus CHIR treatment in U2OS cells. Red dotted line indicates cutoff (*P*-value: 0.05).

**A**

IP

FOXP2 β-catenin control input

FOXP2

β-catenin

**B**

control CHIR

Nuclear fraction — β-catenin / Lamin

Cytosolic fraction — β-catenin / GAPDH

**C**

Upregulated genes

FOXP2+CHIR

1913

1704

427

798

716

499

53

FOXP2

CHIR

Downregulated genes

FOXP2+CHIR

833

1554

337

1795

767

905

301

FOXP2

CHIR

**D**

### Upregulation

| Condition | DEGs | KEGG-pathways |
|---|---|---|
| FOXP2 | 499 | NOD-like receptor signaling pathway, PI3K-Akt signaling pathway, RNA transport, Ribosome biogenesis in eukaryotes, Hippo signaling pathway |
| CHIR | 716 | Ras signaling pathway, Proteaglycans in cancer, Mucin type O-glycan biosynthesis, Cholinergic synapse, Rap1 signaling pathway |
| FOXP2 + CHIR | 1913 | Phagosome, Neuroactive ligand-receptor interaction, Mineral absorption, Prolactin signaling pathway, Synaptic vesicle cycle |
| FOXP2, CHIR | 53 | Pancreatic cancer, Adherens junction, Chronic myeloid leukemia |
| FOXP2, FOXP2 + CHIR | 1704 | Ribosome biogenesis in eukaryotes, RNA transport, TNF signaling pathway, Mineral absorption, Bile secretion |
| CHIR, FOXP2 + CHIR | 427 | Cytokine-cytokine receptor interaction, Protein digestion and absorption, Jak-STAT signaling pathway, Amoebiasis, Inflammatory bowel disease |
| FOXP2, CHIR, FOXP2 +CHIR | 798 | Ribosome biogenesis in eukaryotes, RNA polymerase, Transcriptional misregulation in cancer, Fructose and mannose metabolism, TNF-signaling pathway |

### Downregulation

| Condition | DEGs | KEGG-pathways |
|---|---|---|
| FOXP2 | 905 | Circadian entrainment, Aldosterone synthesis and secretion, Signaling pathways regulating pluripotency of stem cells, Glutamatergic synapse, Cell adhesion molecules |
| CHIR | 767 | Calcium signaling pathway, Neuroactive ligand-receptor interaction, Salivary secretion, Oxytocin signaling pathway, cAMP signaling pathway |
| FOXP2 + CHIR | 833 | Arrhythmogenic right ventricularcyrdiomyopathy, Dilated cardiomyopathy, Focal adhesion, Hepatitis B, Hypertrophic cardiomyopathy |
| FOXP2, CHIR | 301 | cGMP-PKG signaling pathway, Cell adhesion molecules, Tryptophan metabolism, Regulation of lipolysis in adipocytes |
| FOXP2, FOXP2 + CHIR | 1554 | Axon guidance, Hippo signaling pathway, Ether lipid metabolism, Bacterial invasion of epithelial cells, Regulation of actin cytoskeleton |
| CHIR, FOXP2 + CHIR | 337 | PI3K-Akt signaling pathway, Focal adhesion, ECM-receptor interaction, Pathways in cancer, Hepatitis C |
| FOXP2, CHIR, FOXP2 +CHIR | 1795 | Calcium signaling pathway, Hypertrophic cardiomyopathy, PI3K-AKT signaling pathway, Pathways in cancer, Dilated cardiomyopathy |

**E**

Upregulated biological functions

Mitochondrial fission
Visual perception
Cell surface receptor signaling pathway
Mitochondrial translation termination
Transferrin transport
Immune response-inhibiting signaling pathway
Fc receptor mediated inhibitory signaling pathway
Vasoconstriction
Negative regulation of T cell proliferation
Mitochondrial translation elongation
Sodium ion transmembrane transport
Zinc II ion transmembrane transport
B cell homeostasis
Receptor guanylyl cyclase signaling pathway
Response to stimulus

*P*-value

Downregulated biological functions

Mitotic nuclear division
Chromosome segregation
Sister chromatid cohesion
DNA double-strand break processing
Cell division
Developmental growth
Strand displacement
Very long-chain fatty acid metabolic process
Golgi vesicle transport
Endodermal cell differentiation
dAMP biosynthetic process
Mitochondrial transport
Spindle organization
Positive regulation of gene expression
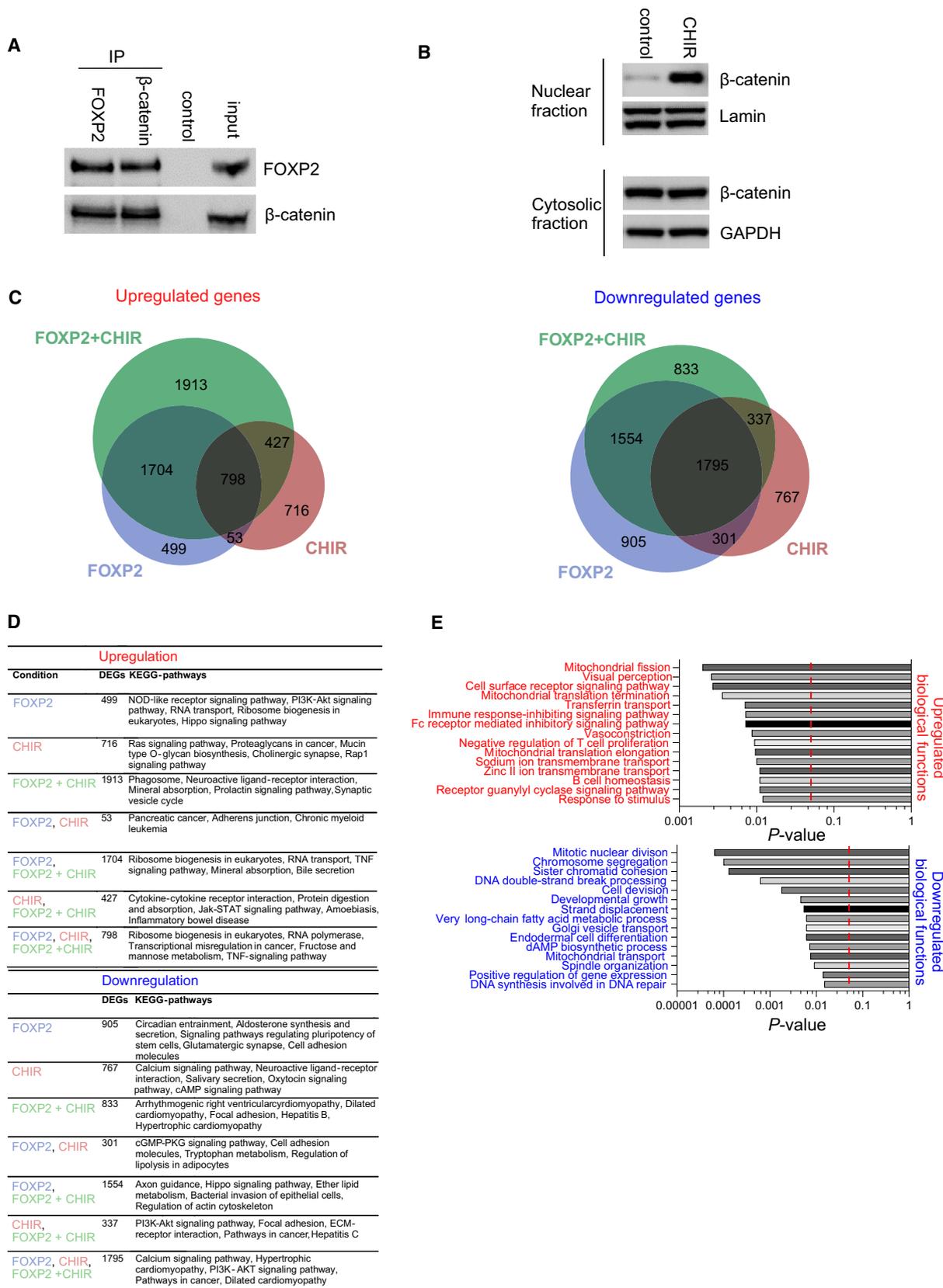DNA synthesis involved in DNA repair

*P*-value

**Fig. 4.** FOXP2 modulates the Wnt pathway. (A) Heatmap of Wnt target genes in FOXP2-overexpressing cells (FOXP2), CHIR-treated cells (CHIR), and FOXP2-overexpressing cells treated with CHIR (FOXP2 + CHIR), genes are represented in a range of red (upregulated) and blue (downregulated) ($n$ = 5). (B) Validation of selection of Wnt targets by qPCR. Data represent the mean $\pm$ SEM, $n$ = 5, two-way ANOVA (Tukey's multiple comparisons test) was performed. $P > 0.05$ = NS; $P < 0.05$ = *; $P < 0.01$ = **; $P < 0.001$ = ***; $P < 0.0001$ = ****. (C) Number of up- and downregulated genes in each condition compared with control cells. (D) FOXP2 siRNA knockdown efficiency validation. All of the four preselected FOXP2 siRNAs could decrease FOXP2 protein expression significantly ($n$ = 1). 'siFOXP2_MIX' is a pool of the four siRNAs. RT–qPCR analysis of *CCND1, TIAM1, JUN, BMP4, CD44,* and *LEF1* mRNA expression upon FOXP2 knockdown and β-catenin activation. Housekeeping gene *HPRT1* was used as reference. siRNA FOXP2_13 was used for FOXP2 knockdown. WNT3a condition medium, GSK inhibitor CHIR, and WNT surrogate were used to active β-catenin. Data represent the mean $\pm$ SEM, $n$ = 3 or 4, two-way ANOVA (Tukey's multiple comparisons test) was performed. $P > 0.05$ = NS; $P < 0.05$ = *; $P < 0.01$ = **; $P < 0.001$ = ***; $P < 0.0001$ = ****.

most up and downregulated genes overlap between the FOXP2 only and FOXP2 plus CHIR conditions, suggesting regulation of FOXP2 function independent of β-catenin/CHIR. The dataset being unique in the condition with FOXP2 overexpression plus CHIR treatment contained 833 genes, which were distributed in eight pathways (KEGG) (top 5 in Fig. 3D) and 36 biological processes (GO term) (top 15 in Fig. 3E), suggesting that those pathways and biological processes are only affected by combined FOXP2 overexpression and CHIR treatment and thus give a clue about a regulatory effect of β-catenin on FOXP2. The expression of Wnt targets in the conditions 'Control', 'FOXP2 overexpression' (FOXP2), 'CHIR treatment' (CHIR), and 'FOXP2 overexpression with CHIR treatment' (FOXP2 + CHIR) is shown in Fig. 4A as heatmap. *BMP4, AXIN2, CCND1, APC2,* and *RUNX2* show a different expression pattern in FOXP2 + CHIR than FOXP2 and CHIR alone, indicating that those genes are indeed affected by the effect of CHIR on FOXP2 activity. Validation of our RNA-Seq data using qPCR on a list of Wnt targets confirmed the effect of CHIR on FOXP2 activity (Fig. 4B).

Moreover, our RNA-Seq data show that β-catenin significantly increases the number of genes upregulated by FOXP2, whereas the number of downregulated genes remains the same compared with FOXP2 overexpression only (Fig. 4C). These results indicate that the FOXP2 repressor function is counteracted by β-catenin, which would happen under conditions of Wnt pathway activation.

To further substantiate the potential link between FOXP2 and Wnt signaling, we carried our qPCR analysis in a different cell line (HEK293T) and using FOXP2 silencing instead of overexpression. Using three different Wnt pathway activators, we reveal that a set of Wnt target genes are regulated in a FOXP2-dependent manner. Moreover, we obtained consistent results for all three Wnt pathway activators tested,

including different concentrations of WNT3a conditioned medium, the Wnt Surrogate-Fc fusion protein, and CHIR (Fig. 4D).

Summarizing, our RNA-Seq and qPCR data show that Wnt signaling, resulting in increased nuclear levels of β-catenin, regulates expression of a set of target genes in a FOXP2-dependent manner.

## Multiple regions in FOXP2 bind to β-catenin in cells and *in vitro*

Interactions of β-catenin with FOXP1 [22] and FOXP3 [23] have been reported recently. However, the molecular details of the interaction of β-catenin with FOXP proteins remain elusive. In order to identify the binding regions of β-catenin on FOXP2, we generated several FOXP2 constructs. FOXP2 consists of four structured domains which are connected with stretches with a high degree of predicted disorder (Fig. 5A). N-terminally, FOXP2 contains a poly-Q region, which generally can function as functional modulator in transcription factors [48]. The folded zinc finger and leucine zipper domains have been shown to mediate protein–DNA interactions and dimerization of FOXP proteins, respectively [49]. The forkhead domain acts as DNA-binding domain and is highly conserved in the FOXP family [1] (Fig. 2).

We designed our constructs by decreasing the protein size progressively regarding its functional domains and regions (Fig. 5B). Respective FOXP2 proteins were tested on their interaction with endogenous β-catenin by coimmunoprecipitation experiments. For this set-up, we used U2OS cells, which contain only endogenous β-catenin and no FOXP2, thus allowing us to examine β-catenin binding to exogenous FOXP2. We overexpressed different FOXP2 constructs in comparable amounts and performed the coimmunoprecipitation using either FOXP2 or β-catenin as bait. In line with FOXP1 and FOXP3, full-length FOXP2 binds to β-catenin (Fig. 6A). Deletion of the poly-Q region
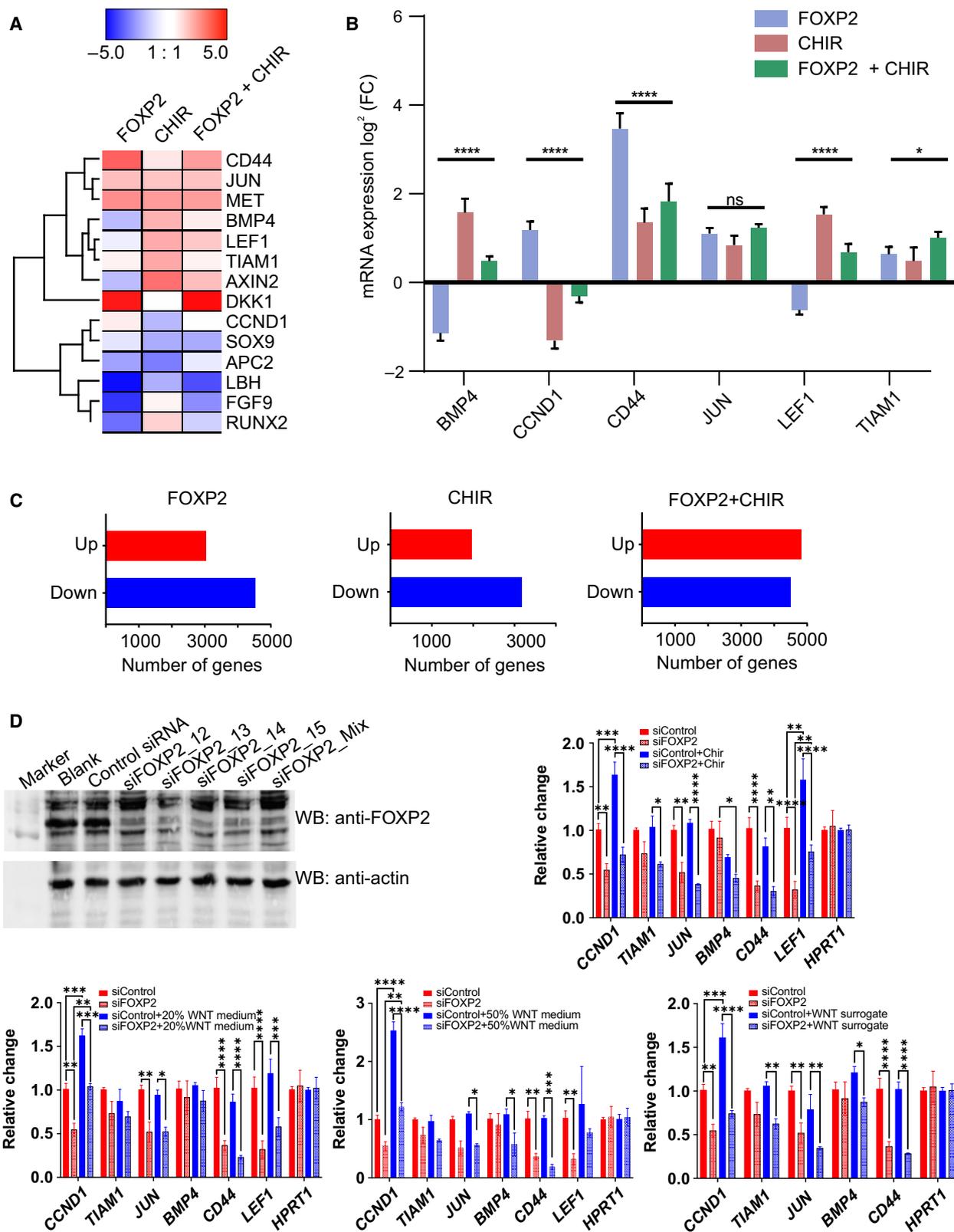
showed similar amounts of coimmunoprecipitated β-catenin compared with the full-length construct, indicating that this region is not involved in FOXP2 binding. In contrast, further deletion of the potentially intrinsically disordered region (IDR) from residue 247 to 341 leads to decreased amounts of bound β-catenin, suggesting that this region is involved in β-catenin binding. Further deletion of the region harboring the zinc finger and leucine zipper (residue 342–503) did not alter the amount of bound β-catenin, suggesting that the C-terminal region containing the forkhead domain and a C-terminal IDR is sufficient for β-catenin binding and constitutes a second binding site. Taken together, those results indicate that both, the FOXP2$^{FH}$ domain and the disordered region, are involved in β-catenin binding.

In order to further validate the direct interaction between β-catenin and FOXP2, the expressed and purified FOXP2 proteins were tested using nuclear magnetic resonance (NMR) spectroscopy. Both FOXP2 (80 kDa) and β-catenin (85 kDa) full-length proteins are challenging for NMR spectroscopy because of severe line broadening and spectral overlap. Thus, we designed two shorter FOXP2 constructs based on our coimmunoprecipitation experiments: (a) the IDR (FOXP2$^{IDR}$, residues 247–341) and (b) the forkhead domain (FOXP2$^{FH}$, residues 504–594) (Fig. 5B).

In line with the Co-IP data, addition of increasing amounts of unlabeled full-length β-catenin to $^{15}$N-labeled FOXP2$^{FH}$ resulted in a progressive disappearance of a set of $^{1}$H,$^{15}$N cross-peaks indicating direct interaction between FOXP2$^{FH}$ and β-catenin (Fig. 6B). To identify the β-catenin regions involved in the interaction with FOXP2$^{FH}$, we carried out additional binding studies.

β-catenin is composed of multiple domains that could be involved in FOXP2 binding. In addition to the folded core region, which is composed of 12 copies of a 42 amino acid sequence motif known as an armadillo repeat, the N- and C-terminal regions are intrinsically disordered [50]. Both, the armadillo repeat region and the disordered termini, have been reported to bind interaction partners [51]. To identify the β-catenin domain(s) involved in the interaction with the FOXP2, we first recorded $^{1}$H,$^{15}$N HSQC NMR spectra of $^{15}$N-labeled FOXP2$^{FH}$ free and in the presence of unlabeled β-catenin N terminus (β-catenin$^{1-140}$), C terminus (β-catenin$^{666-781}$), or a construct containing the N-terminal part of the armadillo region (residues 141–304). Although no binding could be observed for β-catenin$^{141-304}$ (Fig. 6D), both disordered termini showed binding, as indicated by increasing chemical shift perturbations upon addition of increasing amounts of the unlabeled binding partners (Fig. 6C, E). Inspection of the affected residues revealed that both disordered β-catenin regions bind similar regions within FOXP2$^{FH}$, close, but not overlapping with the DNA-binding interface, involving residues located within FOXP2$^{FH}$ α-helices 1, 2, 3, and 4 (Fig. 6F,G).
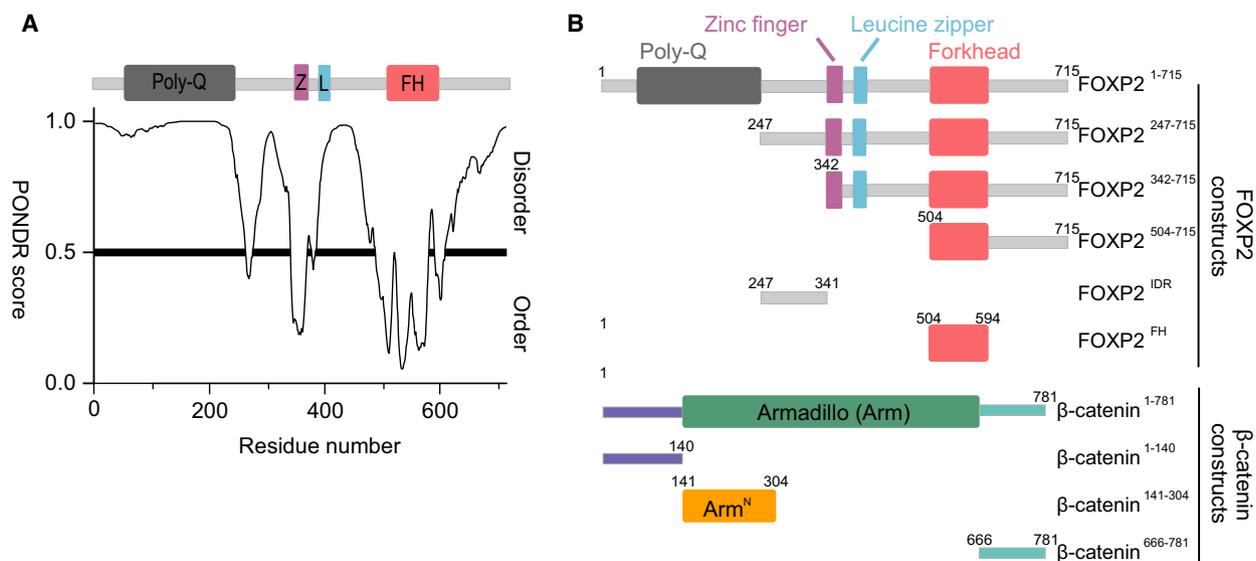


**Fig. 5.** Structural organization of FOXP2 and β-catenin. (A) Disorder prediction using PONDR® (www.pondr.com) for FOXP2 indicating the α-helix around residue 270, zinc finger, leucine zipper, and the forkhead as ordered. (B) Schematic representation of FOXP2 constructs used for cell-based and *in vitro* experiments.
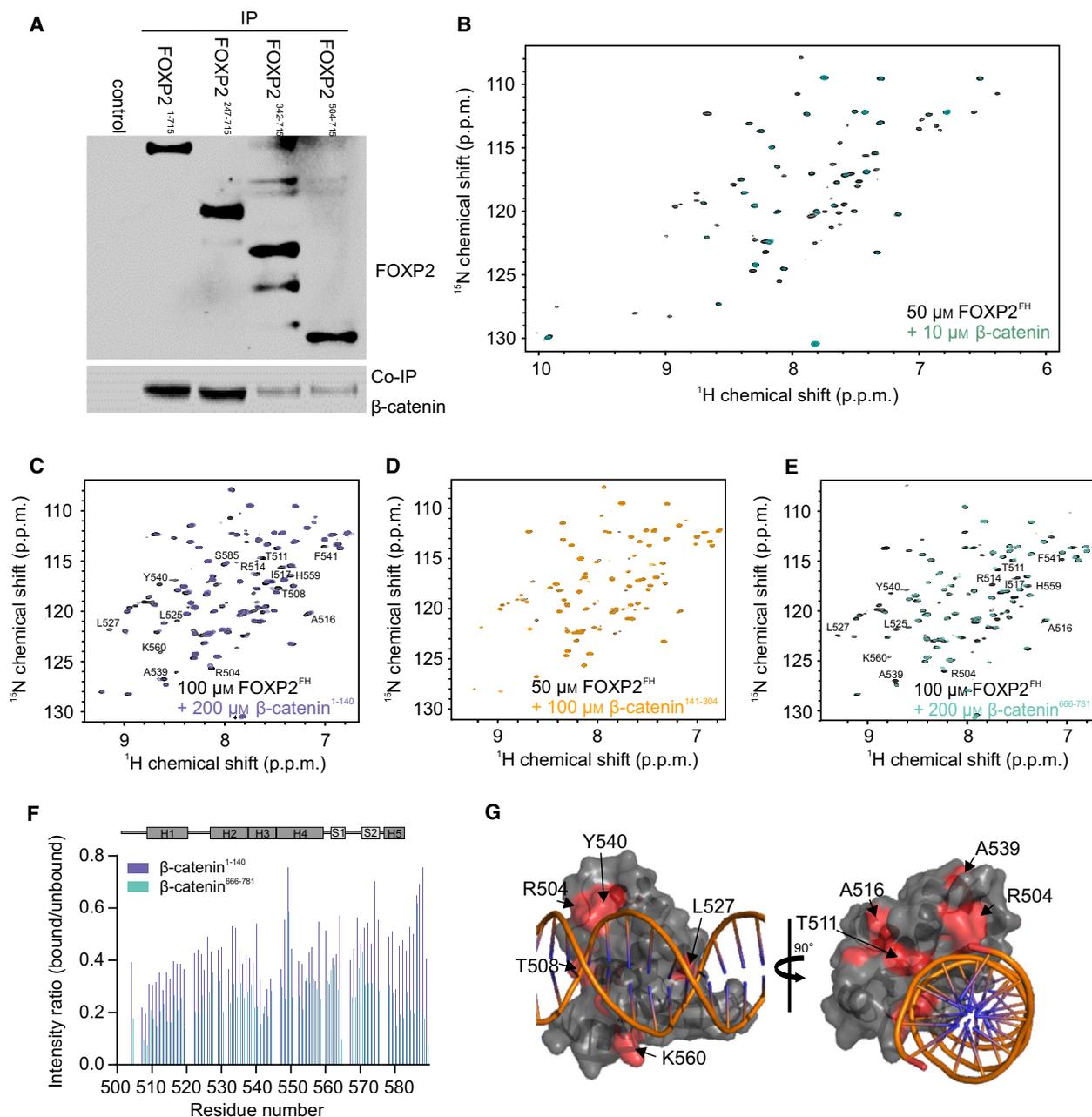
**Fig. 6.** Multiple regions in FOXP2 bind to β-catenin in cells and *in vitro*. (A) Co-IP with FOXP2 constructs and endogenous β-catenin in U2OS cells. (B) $^1$H $^{15}$N HSQC of $^{15}$N labeled FOXP2$^{FH}$ (black) titrated with unlabeled β-catenin (light green) showing the direct interaction of both proteins. (C) $^1$H $^{15}$N HSQC of $^{15}$N labeled FOXP2$^{FH}$ (black) titrated with unlabeled β-catenin$^{1-140}$ (light purple). (D) $^1$H $^{15}$N HSQC of $^{15}$N labeled FOXP2$^{FH}$ (black) titrated with unlabeled β-catenin$^{141-304}$ (orange). (E) $^1$H $^{15}$N HSQC of $^{15}$N labeled FOXP2$^{FH}$ (black) titrated with unlabeled β-catenin$^{666-781}$ (light blue). (F) Intensity plot showing the intensity difference between bound and unbound residues of FOXP2$^{FH}$ and β-catenin$^{1-140}$ and β-catenin$^{666-781}$. Helices and sheets of the forkhead domain are shown as cartoon on top of the plot. (G) Visualization of the binding interface between the N-terminal region of β-catenin (red) and the forkhead (gray) of FOXP2 using the PDB structure (PDB ID 2A07) of the forkhead domain bound to DNA (orange-blue), using The PYMOL MOLECULAR GRAPHICS SYSTEM, version 2.4 (Schrödinger, LLC, New York, NY, USA).

To reveal the molecular details of β-catenin binding to the FOXP2$^{IDR}$, we first characterized the structural features of this region with high degree of predicted disorder. In line with the disorder prediction, the low dispersion of cross-peaks in the $^1$H,$^{15}$N HSQC NMR spectrum, NMR relaxation data, and the NMR

secondary chemical shifts confirm that FOXP2$^{IDR}$ is highly disordered (Fig. 7A,B). Strikingly, a short region with increased α-helical propensity was detected from amino acids 264 to 272, as indicated by NMR

secondary chemical shifts (Fig. 7B, upper panel), decreased flexibility (Fig. 7B, lower panel), and decreased disorder (Fig. 5A). Addition of increasing amounts of unlabeled β-catenin to $^{15}$N-labeled
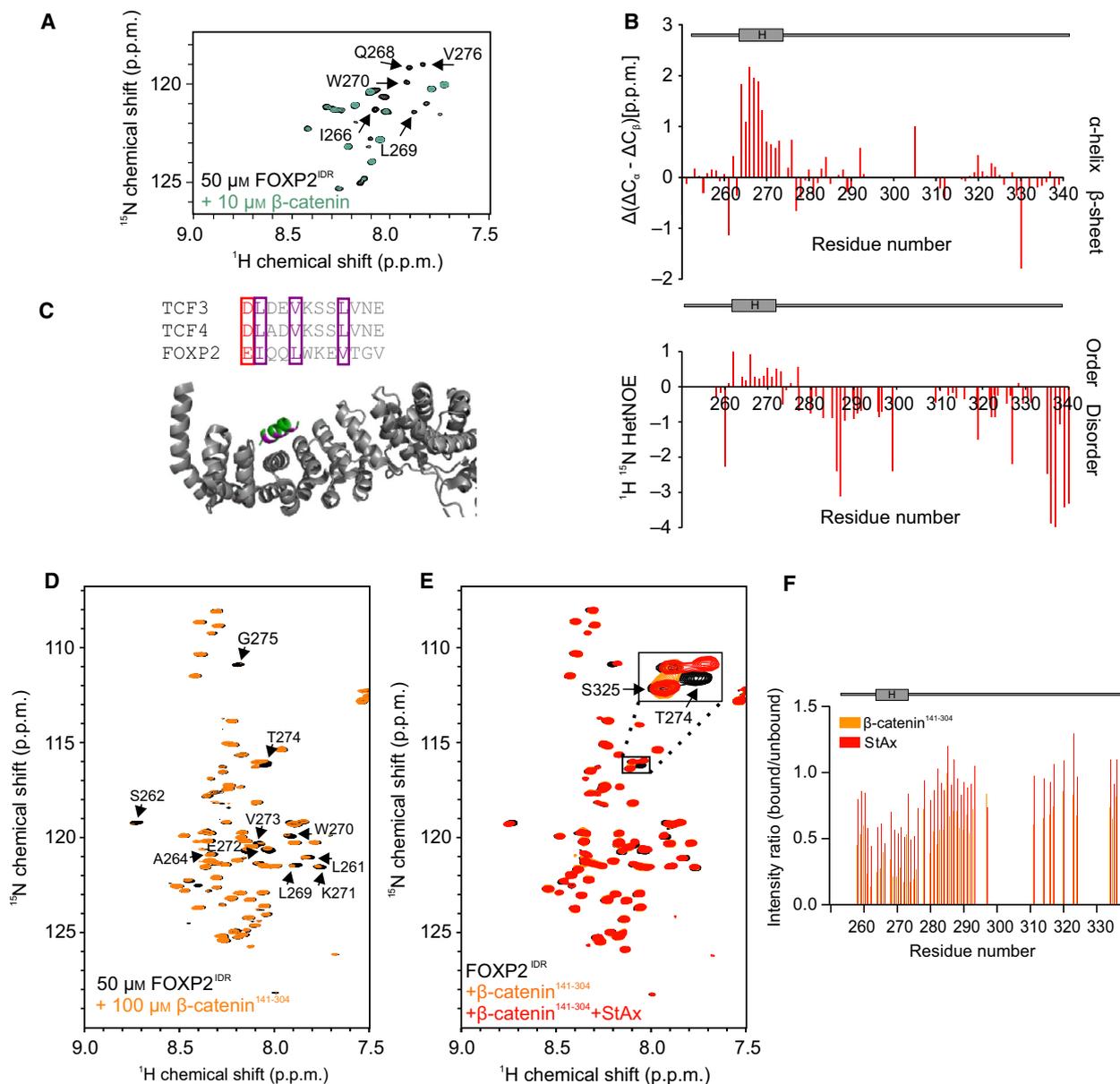


**Fig. 7.** IDR of FOXP2 mediates β-catenin binding. (A) $^1$H $^{15}$N HSQC of $^{15}$N labeled FOXP2$^{IDR}$ titrated with β-catenin showing the direct interaction. (B) Secondary chemical shift perturbations obtained from NMR assignments indicate an α-helical propensity of residue 264–272 in the FOXP2 $^{IDR}$ construct (upper panel). $^{15}$N{$^1$H} heteronuclear NOE of $^{15}$N FOXP2$^{IDR}$ indicating decreased flexible region between residue 265 and 274 (lower panel). (C) Sequence alignment of TCF3 and TCF4 compared to the region with α-helical propensity indicates similar charges and hydrophobicity of residues involved in β-catenin binding. PDB model shows armadillo domain of β-catenin (gray), bound to region of TCF3 (green), residues of TCF3 involved in the binding (magenta), using The PYMOL MOLECULAR GRAPHICS SYSTEM, version 2.4 (Schrödinger, LLC). (D) $^1$H $^{15}$N HSQC of $^{15}$N labeled FOXP2$^{IDR}$ (black) titrated with unlabeled β-catenin$^{141-304}$ (orange). (E) $^1$H $^{15}$N HSQC of $^{15}$N labeled FOXP2$^{IDR}$ (black) titrated with β-catenin$^{141-304}$ (orange) and StAx peptide (red) showing the competition of FOXP2$^{IDR}$ and StAx to same binding side on β-catenin$^{141-304}$. (F) Intensity plot showing the intensity difference between bound and unbound residues of FOXP2$^{IDR}$ versus β-catenin$^{141-304}$ (orange) and the StAx peptide (red).

FOXP2$^{IDR}$ resulted in a progressive disappearance of a set of $^{1}$H,$^{15}$N cross-peaks indicating direct interaction between the FOXP2$^{IDR}$ and β-catenin (Fig. 7A). Strikingly, β-catenin binds to the short α-helical region (residues 262–275). By comparing the amino acid sequence of this FOXP2 region with the sequence of the known β-catenin-binding motif of the Wnt signaling transcription factors TCF7L1 and TCF7L2 (also known as TCF3 and TCF4), we identified similar patterns of hydrophobic and charged residues, with the consensus [D/E]ΦX$_2$ΦX$_3$Φ, where Φ is a hydrophobic residue and X$_2$/X$_3$ is a 2/3-residues spacing between the hydrophobic residues (Fig. 7C). This indicates that the FOXP2$^{IDR}$ binds to β-catenin in a similar orientation as TCF7L1 and TCF7L2. This particular binding site was further validated using different β-catenin constructs and a competition experiment (see below).

To further characterize binding between FOXP2$^{IDR}$ and β-catenin, we recorded $^{1}$H,$^{15}$N HSQC NMR spectra of $^{15}$N-labeled FOXP2$^{IDR}$ free and upon addition of increasing amounts of unlabeled β-catenin$^{141-304}$. A progressive increase was observed in chemical shift perturbations of a set of FOXP2$^{IDR}$ $^{1}$H,$^{15}$N cross-peaks, proving the direct interaction between FOXP2$^{IDR}$ and the N-terminal part of the armadillo domain of β-catenin (Fig. 7D). To reveal the site in β-catenin recognizing the FOXP2$^{IDR}$, and to complement our structural comparison of FOXP2 and TCF7L1/TCF7L2 binding (see above), we carried out competition experiments with the known β-catenin-binding partner StAx (stapled Axin). StAx is a short-stapled peptide derived from the native β-catenin interaction partner tumor suppressor protein Axin-1 and has been reported to bind the N-terminal part of the β-catenin armadillo domain [52]. In line with a competition of StAx and FOXP2$^{IDR}$, addition of increasing amounts of StAx to a preformed complex of $^{15}$N-labeled FOXP2$^{IDR}$ and unlabeled β-catenin$^{141-304}$ leads to a subsequent recovery of FOXP2$^{IDR}$ signal intensity (Fig. 7E,F for reference titrations).

Taken together, this set of experiments suggests that both disordered β-catenin regions are involved in the regulation of FOXP2 activity and specificity to DNA. Both N- and C-terminal β-catenin disordered regions have been proposed to act as transactivation domains and to bind other proteins, such as α-catenin and DVL-1 [53,54]. Thus, we propose that via these interactions additional cofactors regulating transcriptional activity are recruited to FOXP2 via β-catenin.

Summarizing, NMR chemical shift titrations are in line with our Co-IP data and confirm the existence of two distinct β-catenin-binding sites within FOXP2.

Both interaction sites are located on different positions of the protein, which leads to the idea that the IDR might play a crucial role in the regulation of FOXP2 transcriptional activity. It is likely to assume be that this IDR binds to cofactors, such as β-catenin, and facilitates the binding of those to the forkhead domain. Another possibility might be, that the IDR, eventually bound to cofactors, competes with other proteins for binding to the forkhead domain, in turn regulating FOXP2 activity by affecting the DNA affinity.

We could show that β-catenin binds to FOXP2$^{IDR}$ residues harboring a transiently folded α-helix. IDRs are known to play crucial roles in protein–protein interactions. Due to their flexibility, they can adapt to many structurally different interaction partners and form low-affinity complexes, which are important in signaling processes [55]. This novel secondary structure in FOXP2 might constitute a broad interaction site for various interaction partners. Interestingly, the transiently folded α-helix is conserved in FOXP1 and FOXP4 (Fig. 2), indicating a broader function within the FOXP family. Thus, the IDR might play a crucial role in the regulation of FOXP2 activity, as it could enhance or inhibit binding to DNA and other interaction partners and cofactors.

Moreover, the IDR harbors an interesting feature as it contains the two amino acids which differ between chimpanzee and humans [2]. These residues might be crucial for β-catenin binding and therefore for evolutionary development of speech in humans and chimpanzee.

## Deletion of the disordered β-catenin-binding site alters FOXP2 transcriptional activity in the presence and absence of β-catenin

In order to elucidate the role of the FOXP2$^{IDR}$ in transcriptional regulation of FOXP2 target genes in the absence or presence of β-catenin, RNA-Seq analysis was performed. To this end, we designed a FOXP2 full-length construct lacking the α-helical β-catenin-binding region (residue 264–272, further called FOXP2$^{Δhelix}$) for mammalian cell expression.

To analyze the effect of FOXP2 helix deletion in the absence of nuclear β-catenin, we compared the FOXP2 and FOXP2$^{Δhelix}$ RNA-Seq data. Strikingly, we found that 30% of the downregulated and 33% of upregulated genes differ between both conditions (Fig. 8A). Therein, 618 of upregulated genes were unique for FOXP2. The most significant KEGG pathways and biological functions are listed in Fig. 8B and C,
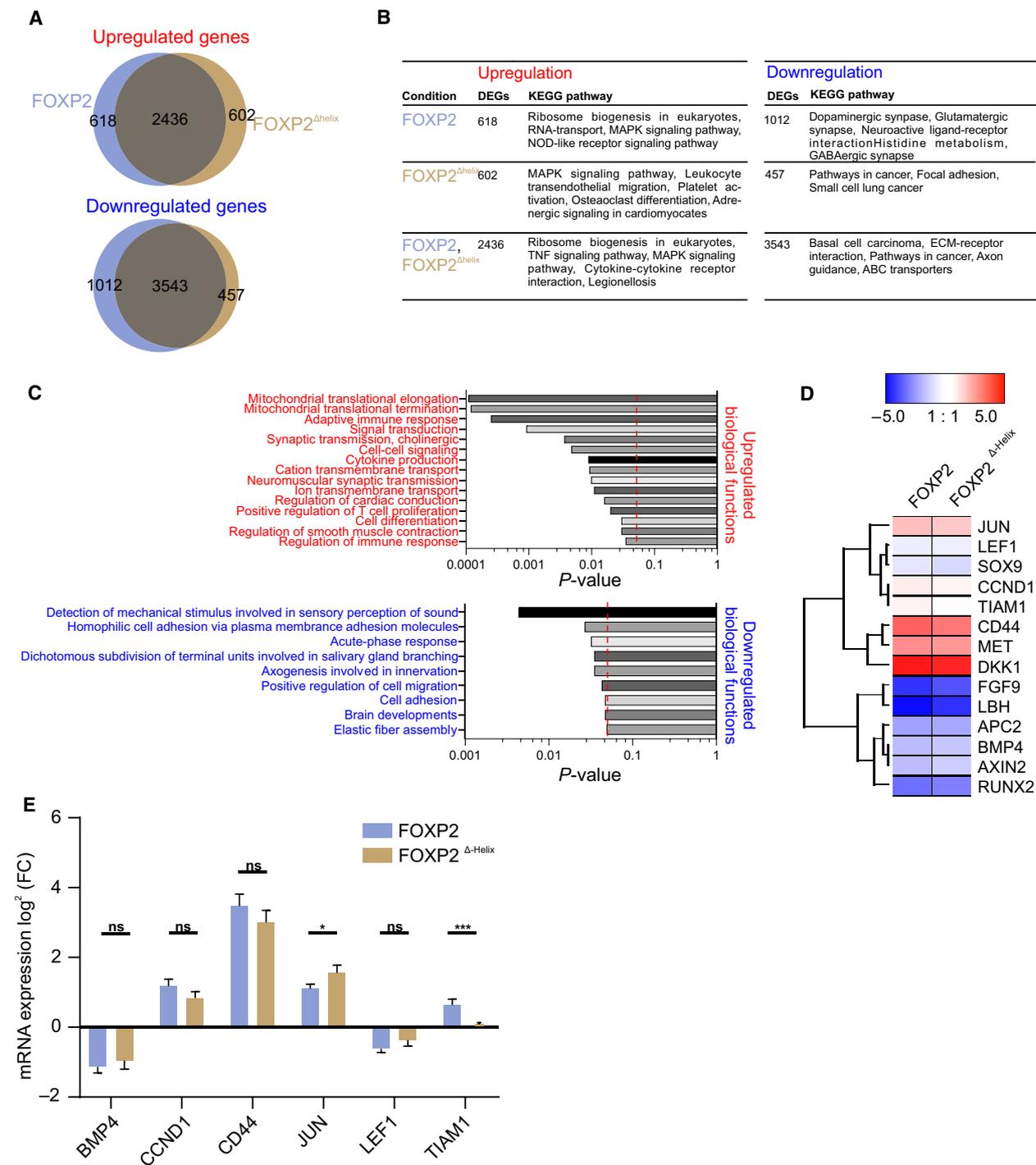
**Fig. 8.** Deletion of the disordered β-catenin-binding site alters FOXP2 transcriptional activity. (A) Venn diagram indicating overlaps of differentially expressed genes in cells overexpressing FOXP2 and FOXP2$^{\Delta\text{-helix}}$. (B) Top 5 of significantly changes KEGG pathways of up- and downregulated genes of each condition of differentially expressed genes. (C) List of significantly enriched GO term biological functions of up- and downregulated genes upon FOXP2$^{\Delta\text{-helix}}$ overexpression in U2OS cells. Red dotted line indicates cutoff (*P*-value: 0.05). (D) Heatmap of Wnt target genes in FOXP2-overexpressing cells (FOXP2) and FOXP2$^{\Delta\text{-helix}}$-expressing cells, genes are represented in a range of red (upregulated) and blue (downregulated) (*n* = 5). (E) Validation of selection of Wnt targets by qPCR. Data represent the mean ± SEM, *n* = 5, two-way ANOVA (Tukey's multiple comparisons test) was performed. *P* > 0.05 = NS; *P* < 0.05 = *; *P* < 0.01 = **; *P* < 0.001 = ***; *P* < 0.0001 = ****.

respectively. Interestingly, one of the biological processes associated with the most upregulated genes in this group was 'signal transduction' (36 genes, *P*-value: $9.2 \times 10^{-4}$), which supports the key role of this α-helical region in FOXP2 regulation. Out of a total of 3656 upregulated genes, 602 were unique for FOXP2$^{\Delta helix}$. From a total of 5012 genes, which were downregulated, 3543 genes were similar in both conditions and 457 unique for FOXP2$^{\Delta helix}$ (Fig. 8A). Moreover, 602 upregulated and 457 downregulated genes were unique for FOXP2$^{\Delta helix}$. Wnt genes were slightly affected by helix deletion (Fig. 8D). In order to validate our RNA-Seq data, qPCR was used on a list of Wnt targets and confirmed the effect of the α-helix on FOXP2 activity (Fig. 8E). Our results indicate that the α-helical region is a key motif for the regulation of FOXP2 activity as the variant lacking this motif shows various differentially regulated genes. Mechanistically, this region might function as interaction site for various cofactors, including β-catenin, thereby regulating FOXP2 transcriptional activity.

To analyze the effect of helix deletion in the presence of nuclear β-catenin, we treated a part of the U2OS cells overexpressing FOXP2$^{\Delta helix}$ with the Wnt/β-catenin pathway activator CHIR (FOXP2$^{\Delta helix}$ + CHIR) and compared the corresponding RNA-Seq data to those obtained under conditions only expressing FOXP2$^{\Delta helix}$ and for cells only treated with CHIR (Fig. 9A). We found 770 of a total gene set of 5849 upregulated genes to be similar in all data sets. Beside this, 1655 genes were unique to 'FOXP2$^{\Delta helix}$ + CHIR', indicating that these genes are dependent on the interaction of FOXP2$^{\Delta helix}$ with β-catenin or the effect of the lacking region with α-helical propensity on the regulation of FOXP2 by β-catenin, as those genes do not change upon FOXP2$^{\Delta helix}$ overexpression or CHIR treatment only. KEGG analysis (Fig. 9B) and GO term analysis (Fig. 9C) revealed that 'FOXP2$^{\Delta helix}$' is involved in different pathways compared with 'FOXP2$^{\Delta -helix}$ + CHIR'. Moreover, the number of DEGs reveals a strong effect of β-catenin on FOXP2 activity, as the number of upregulated genes increased by 61% between 'FOXP2' and 'FOXP2 + CHIR' and by 50% between 'FOXP2$^{\Delta helix}$' and 'FOXP2$^{\Delta helix}$ + CHIR' (Fig. 9D). These data emphasize that the α-helical region is important in the regulation of FOXP2 activity, for example, by recruiting transcriptional cofactors, including β-catenin, to FOXP2. By comparing the DEGs between 'FOXP2 + CHIR' and 'FOXP2$^{\Delta helix}$ + CHIR', we could find various DEGs which differ between both conditions (Fig. 9E). Thus, β-catenin seems to have an enormous impact on the regulation of FOXP2 as we observed many changes between the condition 'FOXP2 + CHIR' treat-

ment and 'FOXP2$^{\Delta helix}$ + CHIR'. However, it is worth mentioning that a β-catenin-independent/GSK inhibition/helix deletion-dependent regulatory processes cannot be excluded. This supports our hypothesis that the IDR, containing the α-helical region indeed affects the interaction to cofactors such as β-catenin. The effect of all investigated conditions on selected Wnt targets is displayed in a heatmap in Fig. 9F. As we observed only minor changes in Wnt-related genes between FOXP2 + CHIR and FOXP2$^{\Delta -helix}$ + CHIR, we analyzed the changes using qPCR and confirmed the impact of the α-helical region on FOXP2-dependent regulation of *CCND1*, *JUN*, and *TIAM1* (Fig. 9G). Moreover, the top 10 DEGs of each condition compared with the control condition indicates different regulations of non-Wnt genes upon deletion of the region with α-helical propensity (Table 1).

In this study, we found the Wnt signaling pathway to be regulated by FOXP2 and discovered a direct interaction between β-catenin and FOXP2 for the first time. The Wnt signaling pathway was studied extensively in correlation with embryonal and cancer development. It has already been shown that a few FOX proteins are related to the Wnt signaling pathway and that some of them (i.e., FOXM1 [56], FOXO3a [57], FOXO4 [28]) interact with a crucial player of this pathway, the transcriptional coactivator β-catenin.

We could map two interaction sites of β-catenin to FOXP2. Both binding sites seem to be important for FOXP2 activity as we observed several changes in regulated pathways if the α-helical-binding site within the FOXP2$^{IDR}$ was lacking. Interestingly, this region is conserved in FOXP1 and FOXP4, indicating an important interaction site for other proteins (Fig. 2).

Thus, we propose that the α-helix in the FOXP2 intrinsically disordered region acts as a recruiter for cofactors (Fig. 10A). Cofactors play crucial roles in signal transduction and regulation of transcription factors [58,59]. This regulatory element seems to be important for β-catenin-dependent regulation of FOXP2, as we found various genes differentially changed upon Wnt/β-catenin pathway activation with CHIR. We show for the first time that β-catenin indeed regulates a member of the FOXP protein family via direct interaction with multiple regions. Our data display the first functional explanation of how β-catenin regulates FOXP proteins and the first proof of direct interactions between both proteins (model in Fig. 10B). This sets the mechanistic base for future studies on the involvement of the FOXP2/β-catenin axis in embryonal development.
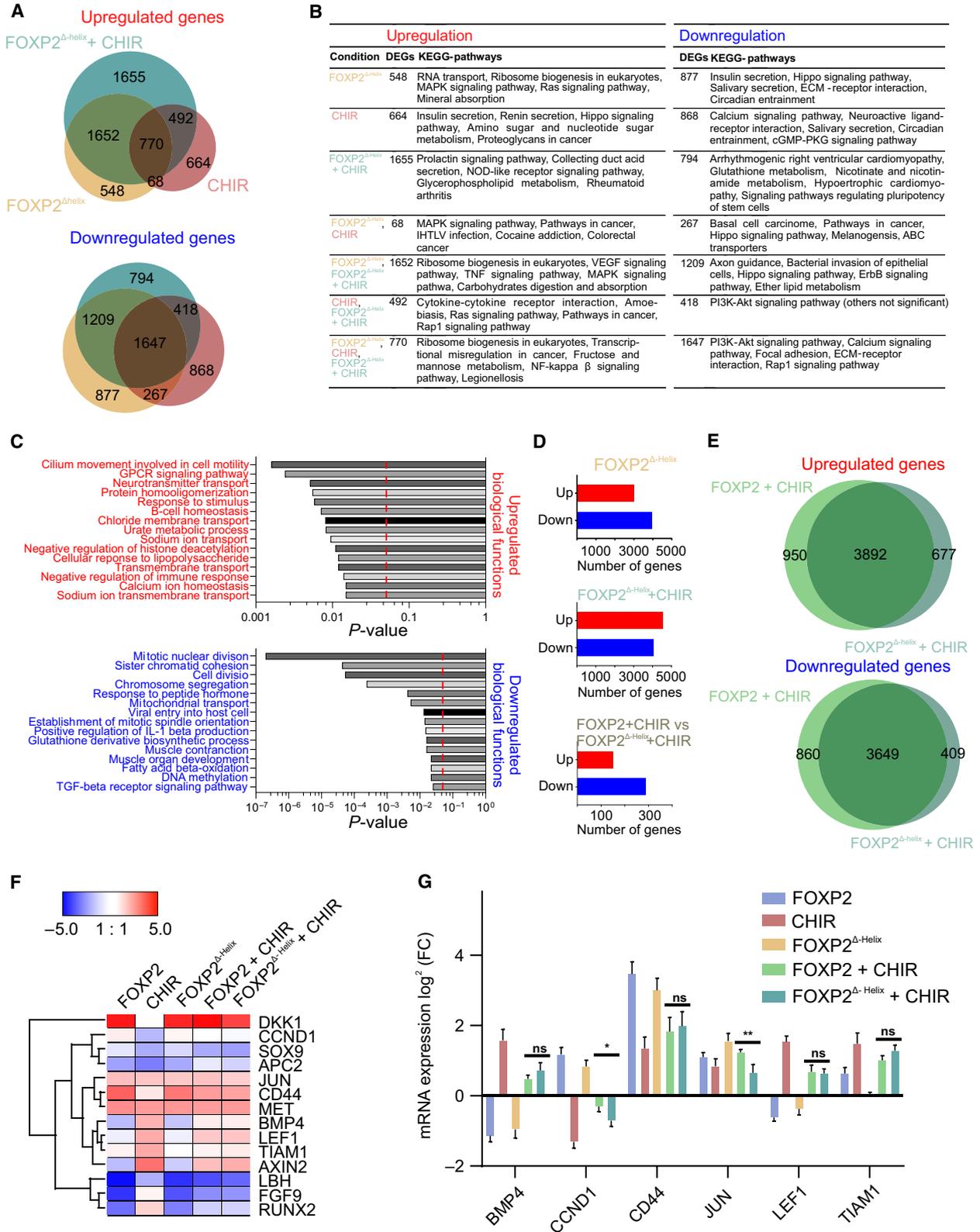
**A** Upregulated genes

FOXP2^Δ-helix + CHIR

Downregulated genes

**B**

| Upregulation | | | Downregulation | | |
|---|---|---|---|---|---|
| Condition | DEGs | KEGG- pathways | | DEGs | KEGG- pathways |
| FOXP2^Δ-Helix | 548 | RNA transport, Ribosome biogenesis in eukaryotes, MAPK signaling pathway, Ras signaling pathway, Mineral absorption | | 877 | Insulin secretion, Hippo signaling pathway, Salivary secretion, ECM -receptor interaction, Circadian entrainment |
| CHIR | 664 | Insulin secretion, Renin secretion, Hippo signaling pathway, Amino sugar and nucleotide sugar metabolism, Proteoglycans in cancer | | 868 | Calcium signaling pathway, Neuroactive ligand-receptor interaction, Salivary secretion, Circadian entrainment, cGMP-PKG signaling pathway |
| FOXP2^Δ-Helix + CHIR | 1655 | Prolactin signaling pathway, Collecting duct acid secretion, NOD-like receptor signaling pathway, Glycerophospholipid metabolism, Rheumatoid arthritis | | 794 | Arrhythmogenic right ventricular cardiomyopathy, Glutathione metabolism, Nicotinate and nicotin-amide metabolism, Hypoertrophic cardiomyo-pathy, Signaling pathways regulating pluripotency of stem cells |
| FOXP2^Δ-Helix, CHIR | 68 | MAPK signaling pathway, Pathways in cancer, IHTLV infection, Cocaine addiction, Colorectal cancer | | 267 | Basal cell carcinome, Pathways in cancer, Hippo signaling pathway, Melanogensis, ABC transporters |
| FOXP2^Δ-Helix, FOXP2^Δ-Helix + CHIR | 1652 | Ribosome biogenesis in eukaryotes, VEGF signaling pathway, TNF signaling pathway, MAPK signaling pathwa, Carbohydrates digestion and absorption | | 1209 | Axon guidance, Bacterial invasion of epithelial cells, Hippo signaling pathway, ErbB signaling pathway, Ether lipid metabolism |
| CHIR, FOXP2^Δ-Helix + CHIR | 492 | Cytokine-cytokine receptor interaction, Amoe-biasis, Ras signaling pathway, Pathways in cancer, Rap1 signaling pathway | | 418 | PI3K-Akt signaling pathway (others not significant) |
| FOXP2^Δ-Helix, CHIR, FOXP2^Δ-Helix + CHIR | 770 | Ribosome biogenesis in eukaryotes, Transcrip-tional misregulation in cancer, Fructose and mannose metabolism, NF-kappa β signaling pathway, Legionellosis | | 1647 | PI3K-Akt signaling pathway, Calcium signaling pathway, Focal adhesion, ECM-receptor interaction, Rap1 signaling pathway |

**C**

**D**

**E**

**F**

**G**

**Fig. 9.** Deletion of the disordered β-catenin-binding site alters FOXP2 transcriptional activity in the presence of β-catenin. (A) Venn diagram indicating overlaps of differentially expressed genes in cells either overexpressing FOXP2$^{\Delta\text{-helix}}$, treated with CHIR and overexpressing FOXP2$^{\Delta\text{-helix}}$ plus CHIR treatment. (B) Top 5 of significantly changes KEGG pathways of up- and downregulated genes of each condition of differentially expressed genes. (C) Top 15 of significantly enriched GO term biological functions of up- and downregulated genes upon FOXP2$^{\Delta\text{-helix}}$ overexpression plus CHIR treatment in U2OS cells. Red dotted line indicates cutoff ($P$-value: 0.05). (D) Number of up- and downregulated genes in each condition compared with control cells. (E) Venn Diagram showing overlaps between conditions 'FOXP2 + CHIR' and 'FOXP2$^{\Delta\text{-helix}}$ + CHIR'. (F) Heatmap of Wnt target genes in FOXP2-overexpressing cells (FOXP2), CHIR-treated cells (CHIR), FOXP2$^{\Delta\text{-helix}}$-overexpressing cells (FOXP2$^{\Delta\text{-helix}}$), FOXP2-expressing cells with CHIR treatment (FOXP2 + CHIR), and FOXP2$^{\Delta\text{-helix}}$-overexpressing cells with CHIR treatment (FOXP2$^{\Delta\text{-helix}}$ + CHIR), genes are represented in a range of red (upregulated) and blue (downregulated) ($n = 5$). (G) Validation of selection of Wnt targets by qPCR. Data represent the mean ± SEM, $n = 5$, two-way ANOVA (Tukey's multiple comparisons test) was performed. $P > 0.05$ = NS; $P < 0.05$ = *; $P < 0.01$ = **; $P < 0.001$ = ***; $P < 0.0001$ = ****.

# Materials and methods

## Plasmids and mutagenesis

Plasmids for human FOXP2 full-length, human FOXP2$^{IDR}$, human β-catenin full-length, human β-catenin$^{1-141}$, human β-catenin$^{141-304}$, and human β-catenin$^{666-781}$ optimized for *Escherichia coli* expression were purchased from Genscript (Piscataway, NJ, USA). Obtained plasmids contained a tobacco etch virus (TEV)-cleavage site following a N-terminal His$_6$- and a protein A-tag for purification. Plasmids containing the FOXP2 full-length optimized for mammalian cell expression were kindly provided from W. Enard (Ludwig Maximilians University Munich, Germany). Truncated variants of FOXP2 were produced by site-directed mutagenesis following the protocol described by Liu and Naismith [60]. The primers were purchased on IDT (Integrated DNA Technology, Inc., Freising, Germany) and used for mutagenesis (listed in Table 2).

## Recombinant protein expression and purification

For the expression of recombinant unlabeled, $^{15}$N or $^{15}$N-$^{13}$C labeled protein, the different bacterial expression vectors were transformed into *E. coli* DE3 strains. Then, a single colony was inoculated in lysogeny broth (LB) medium (20 mL) with kanamycin (25 mg·L$^{-1}$) and cultured at 37 °C until the OD$_{600}$ reached a value between 2 and 3. From this, for unlabeled protein expression, 10 mL was added to 1 L of LB medium with kanamycin (25 mg·L$^{-1}$). For isotope-labeled protein, 1 mL was added to 1 L of $^{15}$N or $^{15}$N-$^{13}$C containing M9 minimal medium, in which $^{15}$N-NH$_4$Cl (1 g·L$^{-1}$) and $^{13}$C-glucose (2 g·L$^{-1}$) for $^{15}$N-$^{13}$C labeled protein and $^{15}$N-NH$_4$Cl (1 g·L$^{-1}$) and $^{12}$C-glucose (4 g·L$^{-1}$) for $^{15}$N labeled protein were the only sources of nitrogen and carbon for NMR isotope labeling purposes (Cambridge Isotope Laboratories, Inc, Tewksbury, MA, USA). Cultures were grown at 37 °C until an OD$_{600}$ of 0.8–1 was reached and then induced with 0.5 mM Isopropyl β-D-1-thiogalactopyranoside (IPTG) followed by protein expression for 16 h at 20 °C. Cells containing disordered

protein constructs such as FOXP2$^{IDR}$, β-catenin$^{1-140}$, and β-catenin$^{666-781}$ were harvested and sonicated in denaturating lysis buffer (50 mM Tris/HCl pH 7.5, 150 mM NaCl, 20 mM Imidazole, 6 M urea), whereas folded protein constructs such as FOXP2$^{FH}$, β-catenin full-length, and β-catenin$^{141-304}$ were harvested and sonicated in nondenaturating lysis buffer (50 mM Tris/HCl pH 7.5, 150 mM NaCl, 20 mM Imidazole, 2 mM Tris(2-carboxyethyl) phosphine (TCEP), 20% glycerol). The cell lysate was separated in soluble and insoluble fraction by centrifugation of the lysate at 33 745 $g$ for 30 min at 4 °C. The soluble His$_6$-tagged protein was purified using Ni-NTA agarose beads (Qiagen, Vienna, Austria), and the His$_6$ tagged protein A-tag was cleaved by TEV protease (5 μg·mL$^{-1}$) incubation over night at 4 °C. Next day, the untagged protein was desalted in Tris-containing buffer (50 mM Tris/HCl pH 7.5, 150 mM NaCl, 20 mM Imidazole, 2 mM TCEP) to remove excessive imidazole from the elution buffer and then separated from the cleaved His$_6$ protein A-tag performing a second affinity purification using Ni-NTA agarose beads. Disordered protein constructs such as FOXP2$^{IDR}$, β-catenin$^{1-140}$, and β-catenin$^{666-781}$ underwent heat shocking at 90 °C for 15 min to minimize protease-induced degradation. A final exclusion chromatography purification step was performed in the buffer of interest on a gel filtration column (Superdex 75; GE Healthcare, Vienna, Austria). Protein concentrations were estimated from their absorbance at 280 nm, assuming that the ε value at 280 nm was equal to the theoretical ε value. The StAx-31 peptide was derived from Boehringer Ingelheim RCV GmbH & CO KG (Vienna, Austria) and synthesized at JPT Peptide Technologies (Berlin, Germany) according to Grossmann *et al.* [52].

## Nuclear magnetic resonance spectroscopy

For protein–protein interaction experiments, $^{15}$N labeled FOXP2$^{IDR}$ and FOXP2$^{FH}$ samples at concentrations of 50–100 μM were prepared in either 50 mM Na$_2$HPO$_4$/NaH$_2$PO$_4$ pH 6.5, 150 mM NaCl, 2 mM β-mercaptoethanol (BME) (Fig. 7D,E) or 50 mM Tris/HCl pH 7.5 (Figs 6B–E and 7A),

**Table 1.** List of most significantly differentially expressed genes in all tested conditions and according to our RNA-Seq data. The fold change is indicated in bracket.

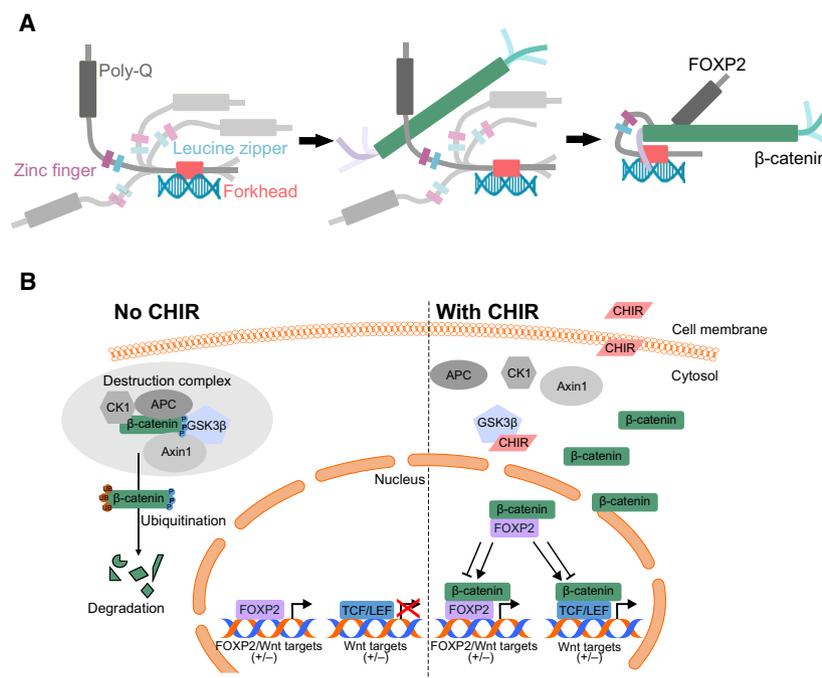| FOXP2 | CHIR | FOXP2^Δhelix | FOXP2 + CHIR | FOXP2^Δhelix + CHIR |
|---|---|---|---|---|
| FOXP2 (13) | GZMB (12) | FOXP2 (12.6) | FOXP2 (14) | FOXP2 (13.8) |
| MMP1 (11.3) | MUCL1 (11.4) | MAL (11.4) | LPAR6 (13) | MAL (12.7) |
| LAPR6 (11.2) | CXCL6 (10.7) | LPAR6 (11.4) | MYCT1 (12.1) | LPAR6 (12.6) |
| CTD-2532D 12.4 (9.4) | MTHFD2P1 (10.7) | MMP1 (10.9) | SERPINB2 (12) | MYCT1 (11.9) |
| MYCT1 (9.3) | C1orf168 (10.1) | MUC5AC (9.7) | RP11-753N 8.1 (11.9) | RP11-753N 8.1 (11.9) |
| IL24 (9) | LINC00161 (9.9) | AGXT (9.5) | SPRR2D (11.3) | MUC5AC (11.6) |
| ENAM (9) | RP11-415C 15.2 (9.8) | MYCT1 (9.4) | CTD-2532D 12.4 (11.2) | AGXT (11.5) |
| AF121898.3 (9) | RP11-95P 13.1 (9.7) | CTD-2532D 12.4 (9.1) | MAL (11.2) | GZMB (11.5) |
| SPRR2D (8.6) | CST1 (9.6) | LINC00659 (9) | MMP1 (10.8) | SERPINB2 (11.1) |
| MAL (8.6) | FILIP1 (9.5) | SRL (8.9) | GZMB (10.8) | SPRR2D (10.7) |
| MMP3 (8.4) | IGFL2 (9.2) | ENAM (8.9) | AC006372.1 (10.7) | MUCL1 (10.5) |
| PRND (−10.5) | MYOCD (−9.2) | PRND (−9.7) | PRND (−10.5) | PRND (−9.2) |
| KANK4 (−9.3) | FOXS1 (−8.8) | PLP1 (−9.7) | SOSTDC1 (−10) | SOSTDC1 (−8.7) |
| HTR2A (−9.2) | NWD1 (−8.5) | KANK4 (−9.1) | IGFBP5 (−9.1) | IGFBP5 (−8.7) |
| SOSTDC1 (−8.9) | GALNT15 (−8.3) | ABCB5 (−8.3) | PLP1 (−8.2) | ABCB5 (−8.3) |
| AC074289.1 (−8.5) | CD180 (−8.1) | CCDC67 (−8) | HTR2A (−8) | APOL4 (−8.2) |
| MYOCD (−8.1) | YPEL4 (−7.9) | CXCL14 (−7.8) | CXCL14 (−8) | GABRR1 (−7.7) |
| CXCL14 (−8.1) | SYT8 (−7.7) | RP11-798L 4.1 (−7.7) | SLC2A12 (−8) | RP1-193H 18.2 (−7.7) |
| FOXS1 (−8) | HRT2A (−7.2) | GABRR1 (−7.7) | AC074289.1 (−7.9) | CXCL14 (−7.7) |
| RP11-798L 4.1 (−7.9) | TNFSF15 (−7.2) | AC074289.1 (−7.6) | R3HDML (−7.8) | GALNT15 (−7.6) |
| ABCB5 (−7.9) | CTD-2334D 19.1 (−6.8) | MYOCD (−7.6) | GALNT15 (−7.6) | FABP7 (−7.6) |
| GABRR1 (−7.9) | LINC00961 (−6.8) | HMGB3P18 (−7.5) | MAP2K6 (−7.5) | KIAA1210 (−7.5) |

**Fig. 10.** Model of FOXP2 function in signal transduction. (A) Schematic model of possible molecular regulatory processes within FOXP2 including the role of the region with α-helical propensity and β-catenin as cofactor. (B) Schematic overview of the effect of CHIR treatment on Wnt signaling pathway and FOXP2 transcriptional activity.

**Table 2.** Primer sequences used for site-directed mutagenesis.

| Constructs | Primer sequences (5′–3′) | Optimized for | Vectors |
|---|---|---|---|
| FOXP2$^{FH}$ | Fw1: CGTCCGCCGTTCACCTAC | *E. coli* cells | pETM11 |
| | Rv1: GGATCCTTATTCCAGGTCTTCTG | | |
| | Fw2: CCCGACGCTGtaaAAAAACATTCC | | |
| | Rv2: GAGCCGGTAATTTTCTGAC | | |
| FOXP2 Construct$^{247–715}$ | Fw: GGCCAGGCAGCACTTCCT | Mammalian cells | pCMV 3Tag |
| | Rv: TTAGGTTTCACAAGTCTCGAGTCATTC | | |
| FOXP2 Construct$^{342–715}$ | Fw: TCTCTATGGCCATGGAGTTT | Mammalian cells | pCMV 3Tag |
| | Rv: AAGCCGAATTCCACCACA | | |
| FOXP2 Construct$^{504–715}$ | Fw: TCAGACCTCCATTTACTTATGC | Mammalian cells | pCMV 3Tag |
| | Rv: AGCCGAATTCCACCACAC | | |
| FOXP2$^{Δhelix}$ | Fw: GTGACTGGAGTTCACAGTATG | Mammalian cells | pCMV 3Tag |
| | Rv: AGGACTTAAGCCAGCTTG | | |

150 mM NaCl and 2 mM TCEP, and 10% D$_2$O for the lock signal. Titrations containing β-catenin full-length were recorded in buffer with pH 7.5, as precipitations occurred at pH 6.5. NMR spectra of FOXP2$^{IDR}$ recorded at pH 7.5 show fewer signals due to different proton exchanges. Therefore, titrations containing $^{15}$N labeled FOXP2$^{IDR}$ and β-catenin$^{141–305}$ (soluble at pH 6.5) were recorded in buffer with pH 6.5. After recording a $^{15}$N HSQC reference spectrum, increasing amounts of the protein partner were added stepwise and $^{15}$N HSQC spectra recorded. If samples were diluted, intensities were normalized by scaling the intensities according to the dilution factor.

For backbone assignment experiments $^{15}$N $^{13}$C labeled FOXP2$^{IDR}$ and FOXP2$^{FH}$ and samples at concentrations of 400–600 μM were prepared in 50 mM Na$_2$HPO$_4$/NaH$_2$PO$_4$ pH 6.5, 150 mM NaCl, 2 mM BME, and 10% D$_2$O for the lock signal. Triple resonance backbone assignment experiments included the following: HNCACB, HN(CO)CACB, HNCO, and HN(CA)CO.

All NMR experiments were performed on a 700 MHz Bruker Avance III NMR spectrometer equipped with a TCI cryoprobe (Bruker Biospin, Rheinstetten, Germany) and a 600 MHz Bruker Avance Neo NMR spectrometer equipped with a TXI 600S3 probe head at 298 K (Bruker Biospin, Rheinstetten, Germany). Spectra were processed using NMRpipe [61] and NMR resonances assigned using CCP NMR [62]. NMR chemical shifts have been submitted to the Biological Magnetic Resonance Bank (BMRB) under the accession numbers BMRB 50427 (FOXP2$^{IDR}$) and BMRB 50426 (FOXP2$^{FH}$).

## Cell culture and transfection

For the Co-IP with endogenous FOXP2 and β-catenin, HEK 293T cells were maintained at 37 °C under 5% $CO_2$ in α-MEM medium (Invitrogen) supplemented with 5% (v/v) FCS (Gibco), 100 $IU·mL^{-1}$ penicillin, and 100 $μg·mL^{-1}$ streptomycin.

U2OS cells were maintained at 37 °C under 5% $CO_2$ in α-MEM medium (Invitrogen, Lofer, Austria) supplemented with 5% (v/v) FCS (Gibco, Thermo Fisher Scientific, Vienna, Austria), 100 $IU·mL^{-1}$ penicillin, and 100 $μg·mL^{-1}$ streptomycin. In a six-well plate, approx. 80% confluent U2OS cells were transfected with various FOXP2 construct plasmids (500 ng) in equal amount using Lipofectamine 3000 (Thermo Fisher Scientific, Vienna, Austria) for 48 h. In case of CHIR treatment, 5 μM CHIR 99021 was added in the medium 72 h before transfection with FOXP2 construct plasmids.

For the qPCR experiments, HEK 293T cells were cultured in DMEM supplemented with 100 $U·mL^{-1}$ penicillin, 100 $mg·mL^{-1}$ streptomycin (Lonza, Basel, Switzerland), and 10% FBS (Lonza, Basel, Switzerland). For FOXP2 knockdown, siRNAs (FlexiTube GeneSolution GS93986 for FOXP2; Qiagen, Vienna, Austria) were transfected to HEK293T cell with Lipofectamine RNAiMAX (Thermo Fisher Scientific, Vienna, Austria) according to manufacturer's instruction. Customized siRNA (Dharmacon, THP Medical Products GmbH, Vienna, Austria, UAGCGACUAAACACAUCAA) was used as a control. For western blot, cells were collected two days after transfection. For RT–qPCR, GSK inhibitor CHIR99021 (final concentration 3 mM) (Sigma-Aldrich, Vienna, Austria), WNT3a conditioned medium (20% or 50%, v/v) (home-made), or Wnt Surrogate-Fc fusion protein (U-protein express) was added to the cells one day after transfection; cells were collected two days after transfection.

## Coimmunoprecipitation

Cells were lysed in lysis buffer [50 mM HEPES, 150 mM NaCl, 1 mM EDTA, 10 mM $Na_4P_2O_7$, 2 mM $Na_3VO_4$, 10 mM NaF, 1% (v/v) Triton X-100, 10% (v/v) glycerol, pH 7.4] containing protease and phosphatase inhibitors (Thermo Fisher Scientific, Vienna, Austria) for 10 min on ice. Cell homogenates were centrifuged at 11292 *g*. (4 °C, 10 min) to pellet debris. Lysates containing equal protein concentrations (1 mg) were precleaned by mixing 20 μL of protein A/G plus agarose (Thermo Scientific) for 2 h at 4 °C followed by centrifugation at 2823 *g*. (4 °C, 5 min) to separate beads. Supernatants were mixed with 1 μg anti-β-catenin or anti-FOXP2 (Cell Signaling, Leiden, The Netherlands - 5337) antibody (BD Biosciences, San Jose, CA, USA - 610154) for 2 h at 4 °C. The immune complexes were precipitated by mixing 20 μL of protein A/G plus agarose

beads overnight at 4 °C. Beads were separated by centrifugation at 10 000 r.p.m. (4 °C, 1 min). After washing three times with a buffer [50 mM HEPES, 300 mM NaCl, 5 mM EDTA, 50 mM NaF, 1% (v/v) Triton X-100, 50 mM Tris/HCl, 0.02% (w/v) $NaN_3$, pH 7.4], beads were resuspended in 40 μL of 4 × NuPAGE LDS sample buffer. Western blot analysis was performed to detect immunoprecipitated β-catenin protein as well as coimmunoprecipitated FOXP2 protein and *vice versa*, as control beads with lysate and without anti-FOXP2/anti-β-catenin antibody were used in order to detect unspecific binding of FOXP2/β-catenin to the beads.

## Western blot analysis

Coimmunoprecipitated proteins (in 4 × NuPAGE LDS sample buffer) or cell lysates were mixed with 4 μL sample reducing agent (Invitrogen) and heated (70 °C, 10 min). Proteins were separated by electrophoresis on a NuPAGE 4–12% Bis-Tris gel and transferred to nitrocellulose membranes (Invitrogen). Membranes were blocked with 5% (w/v) nonfat milk in TBST (Tris-buffered saline containing Tween 20) (25 °C, 2 h) and incubated with anti-β-catenin (BD biosciences-610154, 1 : 2000) or anti-FOXP2 (Cell Signaling-5337, 1 : 1000) antibody [diluted in 5% (w/v) BSA-TBST, overnight at 4 °C]. After washing, membranes were incubated with HRP-conjugated goat anti-mouse IgG (1 : 100 000 Biomol-8101102) or goat anti-rabbit IgG (1 : 200 000 Biomol-6293) (25 °C, 2 h). Immunoreactive bands were visualized using Immobilon Western Chemiluminescent HRP substrate developed by Bio-Rad ChemiDoc MP Imaging System (Millipore, Billerica, MA, USA).

FOXP2 knockdown cells were lysed with sample buffer (0.2% SDS, 10% glycerol, 0.2% 2-mercaptoethanol, 60 mM Tris pH 6.8). Samples were subjected to SDS/PAGE and transferred to PVDF membrane (Merck, Vienna, Austria). Anti-FOXP2 primary antibody (AB-16046; Abcam, Cambridge, UK) and antiactin primary antibody (SC1616; Santa Cruz, Heidelberg, Germany) were used 1 : 5000. Western blot analysis was performed under standard conditions.

## RNA isolation and RNA-Seq

QIAshredder and RNeasy Mini Kit (Qiagen) was used to isolate RNA from transfected U2OS cells according to the manufacturer's protocol. Integrity of RNA was determined using a bioanalyzer instrument (Agilent Technologies, Santa Clara, CA, USA). A cDNA library including five replicates per condition was prepared using the TruSeq Stranded mRNA Sample Prep Kit (Illumina Inc., San Diego, CA, USA) according to the manufacturer's recommendation. Briefly, 1 μg of total RNA was used for first-strand synthesis performed with a random hexamer and SuperScript II (Life Technologies, Carlsbad, CA, USA).

**Table 3.** Primer sequences used for qPCR.

| Gene | Forward primer (5′–3′) | Reverse primer (5′–3′) |
| --- | --- | --- |
| *BMP4* | ATGATTCCTGGTAACCGAATGC | CCCCGTCTCAGGTATCAAACT |
| *CCND1* | GCTGCGAAGTGGAAACCATC | CCTCCTTCTGCACACATTTGAA |
| *CD44* | CTGCCGCTTTGCAGGTGTA | CATTGTGGGCAAGGTGCTATT |
| *HPRT1* | CCTGGCGTCGTGATTAGTGAT | AGACGTTCAGTCCTGTCCATAA |
| *JUN* | TCCAAGTGCCGAAAAGGAAG | CGAGTTCTGAGCTTTCAAGGT |
| *LEF1* | TGCCAAATATGAATAACGACCCA | GAGAAAGTGCTCGTCACTGT |
| *TIAM1* | CCTGTGTCTTACACTGACTCTTC | CATCCCCGTAAAGCCTGCTC |

Second-strand synthesis was performed using dUTP and the Illumina-specific Second Strand Marking Master Mix. After end repair and A-tailing indexed adaptors were ligated to the cDNA fragments. Fragments successfully ligated with adaptor molecules on both ends were enriched by PCR for 15 cycles and purified with AMPure XP Beads (Beckman Coulter Inc., Brea, CA, USA). The final libraries were quality checked on an Agilent Bioanalyzer and quantified with qPCR using a commercially available PhiX-library (Illumina Inc.) as a reference. All samples were run in five biological replicates, and a total of 30 equimolarily pooled samples were sequenced two high output flow cells on an Illumina NextSeq in a paired-end run with $2 \times 75$ cycles. On average, we obtained a mean of 61.7 million reads (range 48.4–87.6) properly paired reads (range 16, 581.904–59 646.128) per sample. Raw RNA-Seq reads were aligned to the human hg19 genome using STAR [63]. Gene read counts are generated using FEATURECOUNTS [64], and differential expression was analyzed using DESEQ2 [65]. Genes with adjusted *P*-value lower than 0.05 and a log2 fold change of 1 or −1 were considered differentially expressed. For pathway analysis, we used DAVID 3.8 [29]. The GO database is currently the most widely used gene annotation system for gene functions and products and provides a better understanding of the links between genes and diseases [66]. The KEGG database, on the other side, combines genetic information with functional information and can thus be used to understand relationships between genes and enriched pathways [67].

### Quantitative real-time PCR (qPCR)

qPCR was performed on 1 μg isolated RNA using the Luna Universal one-step RT–qPCR Kit (New England Biolabs, Frankfurt am Main, Germany) according to the supplier's manual on a 7999HT Fast Real-Time PCR System (Applied Biosystems, Vienna, Austria). The gene-specific primers used for qPCR are listed in Table 3.

Relative gene expression levels were normalized to HPRT1 and calculated using the ΔΔCT method [68] and visualized as log2 fold change. Significance between groups was determined using two-way ANOVA (Tukey's multiple comparisons test) $P > 0.05$ = NS; $P < 0.05$ = *; $P < 0.01$ = **; $P < 0.001$ = ***; $P < 0.0001$ = **** with the software GRAPHPAD PRISM 8.1.1 (GraphPad Software, San Diego, CA, USA, www.graphpad.com).

For qPCR in HEK293T, living cells were harvested in RLT buffer and mRNA was isolated using Qiagen RNeasy Kit (Qiagen). cDNA was synthesized using iScript cDNA synthesis kit (Bio-Rad, Vienna, Austria). SYBR green FastStart master mix (Roche, Vienna, Austria) was used to perform Real-time PCR in the CFX cycler (Bio-Rad). The relative expression level of target genes was normalized to *HPRT1* level (Table 3).

### Conflict of interest

The authors declare no conflict of interest.

### Author contributions

TG, BB, CNK, EM, and DL performed and analyzed cell-based experiments. PU and EH performed RNA-Seq experiments and analysis. GR and BB performed design, expression, and purification of protein constructs, and GR and TM performed NMR experiments and data analysis and wrote the paper.

### Peer Review

The peer review history for this article is available at https://publons.com/publon/10.1111/febs.15656.

# References

1 Lai CS, Fisher SE, Hurst JA, Vargha-Khadem F & Monaco AP (2001) A forkhead-domain gene is mutated in a severe speech and language disorder. *Nature* **413**, 519–523.

2 Enard W, Przeworski M, Fisher SE, Lai CS, Wiebe V, Kitano T, Monaco AP & Paabo S (2002) Molecular evolution of FOXP2, a gene involved in speech and language. *Nature* **418**, 869–872.

3 Shu W, Cho JY, Jiang Y, Zhang M, Weisz D, Elder GA, Schmeidler J, De Gasperi R, Sosa MA, Rabidou D *et al.* (2005) Altered ultrasonic vocalization in mice with a disruption in the Foxp2 gene. *Proc Natl Acad Sci USA* **102**, 9643–9648.

4 Fujita E, Tanabe Y, Shiota A, Ueda M, Suwa K, Momoi MY & Momoi T (2008) Ultrasonic vocalization impairment of Foxp2 (R552H) knockin mice related to speech-language disorder and abnormality of Purkinje cells. *Proc Natl Acad Sci USA* **105**, 3117–3122.

5 Haesler S, Rochefort C, Georgi B, Licznerski P, Osten P & Scharff C (2007) Incomplete and inaccurate vocal imitation after knockdown of FoxP2 in songbird basal ganglia nucleus Area X. *PLoS Biol* **5**, e321.

6 Vernes SC, Oliver PL, Spiteri E, Lockstone HE, Puliyadi R, Taylor JM, Ho J, Mombereau C, Brewer A, Lowy E *et al.* (2011) Foxp2 regulates gene networks implicated in neurite outgrowth in the developing brain. *PLoS Genet* **7**, e1002145.

7 Tsui D, Vessey JP, Tomita H, Kaplan DR & Miller FD (2013) FoxP2 regulates neurogenesis during embryonic cortical development. *J Neurosci* **33**, 244–258.

8 Shu W, Yang H, Zhang L, Lu MM & Morrisey EE (2001) Characterization of a new subfamily of winged-helix/forkhead (Fox) genes that are expressed in the lung and act as transcriptional repressors. *J Biol Chem* **276**, 27488–27497.

9 Vernes SC, Spiteri E, Nicod J, Groszer M, Taylor JM, Davies KE, Geschwind DH & Fisher SE (2007) High-throughput analysis of promoter occupancy reveals direct neural targets of FOXP2, a gene mutated in speech and language disorders. *Am J Hum Genet* **81**, 1232–1250.

10 Spiteri E, Konopka G, Coppola G, Bomar J, Oldham M, Ou J, Vernes SC, Fisher SE, Ren B & Geschwind DH (2007) Identification of the transcriptional targets of FOXP2, a gene linked to speech and language, in developing human brain. *Am J Hum Genet* **81**, 1144–1157.

11 Enard W, Gehre S, Hammerschmidt K, Holter SM, Blass T, Somel M, Bruckner MK, Schreiweis C, Winter C, Sohr R *et al.* (2009) A humanized version of Foxp2 affects cortico-basal ganglia circuits in mice. *Cell* **137**, 961–971.

12 Konopka G, Bomar JM, Winden K, Coppola G, Jonsson ZO, Gao F, Peng S, Preuss TM, Wohlschlegel JA & Geschwind DH (2009) Human-specific transcriptional regulation of CNS development genes by FOXP2. *Nature* **462**, 213–217.

13 Vernes SC, Newbury DF, Abrahams BS, Winchester L, Nicod J, Groszer M, Alarcon M, Oliver PL, Davies KE, Geschwind DH *et al.* (2008) A functional genetic link between distinct developmental language disorders. *N Engl J Med* **359**, 2337–2345.

14 Roll P, Vernes SC, Bruneau N, Cillario J, Ponsole-Lenfant M, Massacrier A, Rudolf G, Khalife M, Hirsch E, Fisher SE *et al.* (2010) Molecular networks implicated in speech-related disorders: FOXP2 regulates the SRPX2/uPAR complex. *Hum Mol Genet* **19**, 4848–4860.

15 Sia GM, Clem RL & Huganir RL (2013) The human language-associated gene SRPX2 regulates synapse formation and vocalization in mice. *Science* **342**, 987–991.

16 Oswald F, Kloble P, Ruland A, Rosenkranz D, Hinz B, Butter F, Ramljak S, Zechner U & Herlyn H (2017) The FOXP2-driven network in developmental disorders and neurodegeneration. *Front Cell Neurosci* **11**, 212.

17 Devanna P, Middelbeek J & Vernes SC (2014) FOXP2 drives neuronal differentiation by interacting with retinoic acid signaling pathways. *Front Cell Neurosci* **8**, 305.

18 Lam EW, Brosens JJ, Gomes AR & Koo CY (2013) Forkhead box proteins: tuning forks for transcriptional harmony. *Nat Rev Cancer* **13**, 482–495.

19 Fisher SE, Vargha-Khadem F, Watkins KE, Monaco AP & Pembrey ME (1998) Localisation of a gene implicated in a severe speech and language disorder. *Nat Genet* **18**, 168–170.

20 Wassink TH, Piven J, Vieland VJ, Pietila J, Goedken RJ, Folstein SE & Sheffield VC (2002) Evaluation of FOXP2 as an autism susceptibility gene. *Am J Med Genet* **114**, 566–569.

21 Herrero MJ & Gitton Y (2018) The untold stories of the speech gene, the FOXP2 cancer gene. *Genes Cancer* **9**, 11–38.

22 Walker MP, Stopford CM, Cederlund M, Fang F, Jahn C, Rabinowitz AD, Goldfarb D, Graham DM, Yan F, Deal AM *et al.* (2015) FOXP1 potentiates Wnt/beta-catenin signaling in diffuse large B cell lymphoma. *Sci Signal* **8**, ra12.

23 Yang S, Liu Y, Li MY, Ng CSH, Yang SL, Wang S, Zou C, Dong Y, Du J, Long X *et al.* (2017) FOXP3 promotes tumor growth and metastasis by activating Wnt/beta-catenin signaling pathway and EMT in non-small cell lung cancer. *Mol Cancer* **16**, 124.

24 Behrens J, von Kries JP, Kuhl M, Bruhn L, Wedlich D, Grosschedl R & Birchmeier W (1996) Functional interaction of beta-catenin with the transcription factor LEF-1. *Nature* **382**, 638–642.

25 Huber O, Korn R, McLaughlin J, Ohsugi M, Herrmann BG & Kemler R (1996) Nuclear localization of beta-catenin by interaction with transcription factor LEF-1. *Mech Dev* **59**, 3–10.

26 Brunner E, Peter O, Schweizer L & Basler K (1997) Pangolin encodes a Lef-1 homologue that acts downstream of Armadillo to transduce the Wingless signal in Drosophila. *Nature* **385**, 829–833.

27 Kaidi A, Williams AC & Paraskeva C (2007) Interaction between beta-catenin and HIF-1 promotes cellular adaptation to hypoxia. *Nat Cell Biol* **9**, 210–217.

28 Essers MA, de Vries-Smits LM, Barker N, Polderman PE, Burgering BM & Korswagen HC (2005) Functional interaction between beta-catenin and FOXO in oxidative stress signaling. *Science* **308**, 1181–1184.

29 da Huang W, Sherman BT & Lempicki RA (2009) Systematic and integrative analysis of large gene lists using DAVID bioinformatics resources. *Nat Protoc* **4**, 44–57.

30 Washbourne P, Dityatev A, Scheiffele P, Biederer T, Weiner JA, Christopherson KS & El-Husseini A (2004) Cell adhesion molecules in synapse formation. *J Neurosci* **24**, 9244–9249.

31 Ardestani A, Lupse B & Maedler K (2018) Hippo signaling: key emerging pathway in cellular and whole-body metabolism. *Trends Endocrinol Metab* **29**, 492–509.

32 Misra JR & Irvine KD (2018) The Hippo signaling network and its biological functions. *Annu Rev Genet* **52**, 65–87.

33 Varelas X, Miller BW, Sopko R, Song S, Gregorieff A, Fellouse FA, Sakuma R, Pawson T, Hunziker W, McNeill H *et al.* (2010) The Hippo pathway regulates Wnt/beta-catenin signaling. *Dev Cell* **18**, 579–591.

34 Legler DF, Micheau O, Doucey MA, Tschopp J & Bron C (2003) Recruitment of TNF receptor 1 to lipid rafts is essential for TNFalpha-mediated NF-kappaB activation. *Immunity* **18**, 655–664.

35 Micheau O & Tschopp J (2003) Induction of TNF receptor I-mediated apoptosis via two sequential signaling complexes. *Cell* **114**, 181–190.

36 Karin M (2005) Inflammation-activated protein kinases as targets for drug development. *Proc Am Thorac Soc* **2**, 386–390; discussion 394–5.

37 Bettelli E, Dastrange M & Oukka M (2005) Foxp3 interacts with nuclear factor of activated T cells and NF-kappa B to repress cytokine gene expression and effector functions of T helper cells. *Proc Natl Acad Sci USA* **102**, 5138–5143.

38 Martin BL & Kimelman D (2009) Wnt signaling and the evolution of embryonic posterior development. *Curr Biol* **19**, R215–R219.

39 Clevers H (2006) Wnt/beta-catenin signaling in development and disease. *Cell* **127**, 469–480.

40 van Amerongen R & Nusse R (2009) Towards an integrated view of Wnt signaling in development. *Development* **136**, 3205–3214.

41 Nusse R & Clevers H (2017) Wnt/beta-catenin signaling, disease, and emerging therapeutic modalities. *Cell* **169**, 985–999.

42 Logan CY & Nusse R (2004) The Wnt signaling pathway in development and disease. *Annu Rev Cell Dev Biol* **20**, 781–810.

43 Reya T & Clevers H (2005) Wnt signalling in stem cells and cancer. *Nature* **434**, 843–850.

44 Zhan T, Rindtorff N & Boutros M (2017) Wnt signaling in cancer. *Oncogene* **36**, 1461–1473.

45 Sumida T, Lincoln MR, Ukeje CM, Rodriguez DM, Akazawa H, Noda T, Naito AT, Komuro I, Dominguez-Villar M & Hafler DA (2018) Activated β-catenin in Foxp3+ regulatory T cells links inflammatory environments to autoimmunity. *Nat Immunol* **19**, 1391–1402.

46 Gottardi CJ & Gumbiner BM (2004) Distinct molecular forms of beta-catenin are targeted to adhesive or transcriptional complexes. *J Cell Biol* **167**, 339–349.

47 de Carvalho A, Strikoudis A, Liu HY, Chen YW, Dantas TJ, Vallee RB, Correia-Pinto J & Snoeck HW (2019) Glycogen synthase kinase 3 induces multilineage maturation of human pluripotent stem cell-derived lung progenitors in 3D culture. *Development* **146**, dev171652.

48 Gemayel R, Chavali S, Pougach K, Legendre M, Zhu B, Boeynaems S, van der Zande E, Gevaert K, Rousseau F, Schymkowitz J *et al.* (2015) Variable glutamine-rich repeats modulate transcription factor activity. *Mol Cell* **59**, 615–627.

49 Li S, Weidenfeld J & Morrisey EE (2004) Transcriptional and DNA binding activity of the Foxp1/2/4 family is modulated by heterotypic and homotypic protein interactions. *Mol Cell Biol* **24**, 809–822.

50 Xing Y, Takemaru K, Liu J, Berndt JD, Zheng JJ, Moon RT & Xu W (2008) Crystal structure of a full-length beta-catenin. *Structure* **16**, 478–487.

51 Valenta T, Hausmann G & Basler K (2012) The many faces and functions of beta-catenin. *EMBO J* **31**, 2714–2736.

52 Grossmann TN, Yeh JT, Bowman BR, Chu Q, Moellering RE & Verdine GL (2012) Inhibition of oncogenic Wnt signaling through direct targeting of beta-catenin. *Proc Natl Acad Sci USA* **109**, 17942–17947.

53 Castano J, Raurell I, Piedra JA, Miravet S, Dunach M & Garcia de Herreros A (2002) Beta-catenin N- and C-terminal tails modulate the coordinated binding of adherens junction proteins to beta-catenin. *J Biol Chem* **277**, 31541–31550.

54 Gujral TS, Karp ES, Chan M, Chang BH & MacBeath G (2013) Family-wide investigation of PDZ domain-mediated protein-protein interactions implicates

beta-catenin in maintaining the integrity of tight junctions. *Chem Biol* **20**, 816–827.

55 Perovic V, Sumonja N, Marsh LA, Radovanovic S, Vukicevic M, Roberts SGE & Veljkovic N (2018) IDPpi: protein-protein interaction analyses of human intrinsically disordered proteins. *Sci Rep* **8**, 10563.

56 Zhang N, Wei P, Gong A, Chiu WT, Lee HT, Colman H, Huang H, Xue J, Liu M, Wang Y *et al.* (2011) FoxM1 promotes beta-catenin nuclear localization and controls Wnt target-gene expression and glioma tumorigenesis. *Cancer Cell* **20**, 427–442.

57 Liu H, Yin J, Wang H, Jiang G, Deng M, Zhang G, Bu X, Cai S, Du J & He Z (2015) FOXO3a modulates WNT/beta-catenin signaling and suppresses epithelial-to-mesenchymal transition in prostate cancer cells. *Cell Signal* **27**, 510–518.

58 Reiter F, Wienerroither S & Stark A (2017) Combinatorial function of transcription factors and cofactors. *Curr Opin Genet Dev* **43**, 73–81.

59 Glass CK & Rosenfeld MG (2000) The coregulator exchange in transcriptional functions of nuclear receptors. *Genes Dev* **14**, 121–141.

60 Liu H & Naismith JH (2008) An efficient one-step site-directed deletion, insertion, single and multiple-site plasmid mutagenesis protocol. *BMC Biotechnol* **8**, 91.

61 Delaglio F, Grzesiek S, Vuister GW, Zhu G, Pfeifer J & Bax A (1995) NMRPipe: a multidimensional spectral processing system based on UNIX pipes. *J Biomol NMR* **6**, 277–293.

62 Vranken WF, Boucher W, Stevens TJ, Fogh RH, Pajon A, Llinas M, Ulrich EL, Markley JL, Ionides J & Laue ED (2005) The CCPN data model for NMR spectroscopy: development of a software pipeline. *Proteins* **59**, 687–696.

63 Dobin A, Davis CA, Schlesinger F, Drenkow J, Zaleski C, Jha S, Batut P, Chaisson M & Gingeras TR (2013) STAR: ultrafast universal RNA-seq aligner. *Bioinformatics* **29**, 15–21.

64 Liao Y, Smyth GK & Shi W (2014) featureCounts: an efficient general purpose program for assigning sequence reads to genomic features. *Bioinformatics* **30**, 923–930.

65 Love MI, Huber W & Anders S (2014) Moderated estimation of fold change and dispersion for RNA-seq data with DESeq2. *Genome Biol* **15**, 550.

66 Jelier R, Goeman JJ, Hettne KM, Schuemie MJ, den Dunnen JT & t Hoen PA (2011) Literature-aided interpretation of gene expression data with the weighted global test. *Brief Bioinform* **12**, 518–529.

67 Kanehisa M, Goto S, Sato Y, Furumichi M & Tanabe M (2012) KEGG for integration and interpretation of large-scale molecular data sets. *Nucleic Acids Res* **40**, D109–D114.

68 Livak KJ & Schmittgen TD (2001) Analysis of relative gene expression data using real-time quantitative PCR and the 2(-Delta Delta C(T)) method. *Methods* **25**, 402–408.